Chapter 7
Locomotion Through Complex Fluids: An Experimental View

Josué Sznitman and Paulo E. Arratia

Abstract Recently, there has been renewed interest in the swimming of microorganisms for applications that include artificial swimmers, novel materials, drug delivery, and micro-robotics. Due to small length scales, the fluid mechanics of swimming of microorganisms are governed by low Reynolds number hydrodynamics. In such a regime, linear viscous forces dominate over nonlinear inertial forces. While our current understanding of locomotion at low Reynolds numbers is derived mainly from investigations in simple, Newtonian fluids (e.g., water), many of the fluids in which locomotion occurs contain solids and/or (biological) polymers that are instead not Newtonian. Examples include wet soils, human mucus, and fluids in the cervix and female reproductive track. A major challenge is to understand the propulsion mechanisms in fluids that display complex rheological behavior such as viscoelasticity and shear-thinning viscosity. Here, we will briefly review a few notable swimming experiments in Newtonian fluids and then discuss the latest experimental results on swimming in complex fluids, focusing on viscoelastic fluids.

1 Introduction

Microorganisms are surrounded by fluids. They cope and take advantage of water or wind currents to move, feed, and reproduce. Many, if not most, living organisms live in the realm of low Reynolds numbers [1], usually defined as $\mathrm{Re} = \rho UL/\mu$, where U is a characteristic speed, L a characteristic length (e.g., body size), and ρ and μ are the fluid's density and dynamic viscosity, respectively. For example, the typical Reynolds number for microorganisms such as eukaryotic protozoa

J. Sznitman (✉)
Department of Biomedical Engineering, Technion-Israel Institute of Technology, Haifa, 32000, Israel
e-mail: sznitman@bm.technion.ac.il

P.E. Arratia
Department of Mechanical Engineering and Applied Mechanics, University of Pennsylvania, Philadelphia, PA 19104, USA
e-mail: parratia@seas.upenn.edu

S.E. Spagnolie (ed.), *Complex Fluids in Biological Systems*, Biological and Medical Physics, Biomedical Engineering,
DOI 10.1007/978-1-4939-2065-5_7

(e.g., sperm cells [2–4]), prokaryotes (e.g., bacteria [5]), and even multicellular organisms (e.g., nematodes [5–7]) is much less than unity ($\mathrm{Re} \ll 1$) due to the organism's small length scale L. By contrast, humans when swimming in the ocean or water pools can reach Reynolds numbers of approximately 10^4. This means that humans can take advantage of nonlinear inertial forces for propulsion, while microorganisms simply cannot. Small living organisms instead have to overcome the linear viscous forces and drag arising from the fluid in order to achieve any appreciable net motion. The picture that emerges is that moving (and living) at low Reynolds number is drastically different from what we (humans) are accustomed to experience in our everyday lives. For the case of swimming microorganisms in simple fluids such as water, the equations of fluid motion become time-reversible (for a more in-depth discussion on the governing equations, please see Chap. 1). As a result, net locomotion can only be generated from nonreciprocal kinematics in order to break time-reversal symmetry [2,8,9]; this is also known as the "scallop theorem" [1] which states that organisms that rely on reciprocal motion for locomotion cannot achieve net motion in the limit of vanishing Reynolds numbers. A more detailed discussion on the scallop theorem is given in Chap. 8.

Microorganisms have developed diverse strategies to break time-symmetry and create nonreciprocal motion (see Fig. 7.1). Such strategies include body undulations and the presence of moving flagella. For example, the motility of various multicellular organisms including the worm nematode *Caenorhabditis elegans* originates from the propagation of undulatory waves from head to tail as a result of patterns of muscle activation and neuromuscular control [10–12]. Locomotion may also result from flagellar motility where one or several bundled appendages protrude from the cell body of certain prokaryotic and eukaryotic cells. One can typically distinguish between bacterial flagella that are helical filaments (e.g., *Escherichia coli* [13–16]) and eukaryotic flagella that are flexible filaments undergoing "whiplike" motions resulting from the action of molecular motors distributed along the filament length; this latter mode of flagellar actuation is seen for example in many sperm cells [17–19]. Other eukaryotic organisms (e.g., *Paramecium*) have instead their body surface covered with thousands of small hairlike protrusions (*cilia*) that beat in a coordinated manner [17, 20].

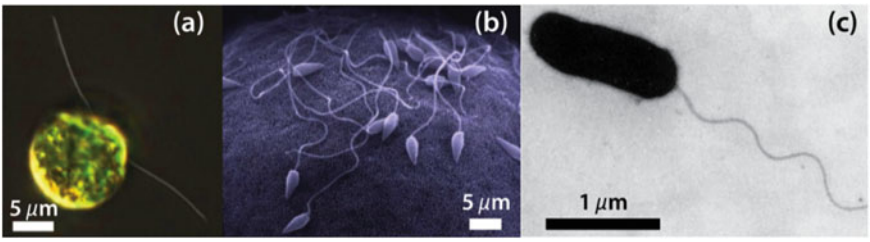

Fig. 7.1 Examples of microorganisms. (**a**) The green algae *Chlamydomonas reinhardtii*, a model eukaryotic organism, (**b**) sperm cells moving next to boundaries, and (**c**) the bacterium *E. coli*, one of the most widely studied prokaryotic model organisms

There are many other cellular environments that are characterized by low Reynolds number locomotion. In mammals, for instance, cells featuring motile cilia include the epithelium of the female Fallopian tubes, where rhythmic beating guarantees translocation of the ovum from the ovary into the uterus [21–23]. Motile cilia are also found in the epithelial lining of the tracheobronchial airways of the lungs [24]. There, the ciliated epithelium prevents mucus accumulation in the airway lumen and serves as an immune barrier against pathogens and foreign particulate matter by the action of the so-called mucociliary escalator [25, 26] characterized by synchronous waves of ciliary beating. These waves effectively transport mucus secretions towards the laryngopharynx for expectoration or swallowing to the stomach.

It is clear from everyday observation and from the few examples cited above that nature has found many fascinating ways to break time-reversibility and achieve net motion at the microscopic scale. And thanks to theoretical, numerical, and experimental investigations, our understanding of swimming of microorganisms at low Reynolds numbers has significantly improved in the past 60 years or so [1,3,8,9,13,27–30]. While much of our efforts have been restricted to swimming in simple, Newtonian fluids (e.g., water), there are many microorganisms that live in (complex) fluids that contain particulates and/or polymers (e.g., human mucus, blood, wet soil, gels, and tissues) and are not Newtonian. Such fluids often possess complex (non-Newtonian) rheological behavior such as shear-thinning viscosity and viscoelasticity. One may expect that swimming in complex fluids such as mucus to be markedly different from swimming in water. But is it? Is swimming in complex fluids at low Reynolds numbers still dominated by purely viscous effects? Does fluid elasticity matter at low Reynolds numbers? Here, we will try to address those questions by examining the recent experimental investigation of swimming of microorganisms in both Newtonian and complex fluids. This chapter is organized as follows: (i) a brief introduction is given on swimming at low Reynolds numbers in simple, Newtonian fluids, (ii) experiments in Newtonian fluids are discussed, (iii) a brief discussion of locomotion in complex fluids is given, (iv) experiments in viscoelastic fluids are discussed, and (v) conclusions and outlook are provided. We begin by introducing some basic principles of swimming at low Reynolds numbers in Newtonian fluids; we note that a more detailed discussion on the basic principles of locomotion in Newtonian and complex fluids can be found in Chaps. 1 and 8.

2 Basic Principles: Fluid Dynamics of Swimming at Low Reynolds Number

Let us begin our discussion of swimming of microorganisms by estimating the Reynolds numbers of the bacterium *E. coli* in water. The shear viscosity μ of water is $1\,\mathrm{mPa}\cdot\mathrm{s}$ (or 1 cP) and independent of shear rate (i.e., Newtonian). The characteristic size L of *E. coli* is approximately $2\,\mu\mathrm{m}$, and the bacterium is known

to achieve net swimming speeds U of approximately $25\,\mu\text{m/s}$ [31]. Following these parameters, we can estimate the Reynolds number for *E. coli* to be approximately $\text{Re} = \rho UL/\mu = 5 \times 10^{-5} \ll 1$, where ρ is fluid density ($10^3\,\text{kg/m}^3$). Such low value of Re implies that linear viscous forces dominate over inertial forces, and the nonlinear convective term in the Navier–Stokes equation can be safely ignored (see Chap. 1). Additionally, one can compute the frequency-based Reynolds number, typically defined as $\text{Re}_{\text{freq}} = \rho L^2 \omega/\mu$, to assess unsteady flow effects, where ω is the frequency at which the bacterium flagella rotate ($\sim 100\,\text{Hz}$). We find again for *E. coli* that $\text{Re}_{\text{freq}} \ll 0.1$, and thus one can assume the flow to be steady. Under those conditions and assuming that the bacterium is moving in an incompressible ($\nabla \cdot \mathbf{u} = 0$), Newtonian fluid (and ignoring body forces like gravity), the equation of fluid motion reduces to

$$\nabla p = \mu \nabla^2 \mathbf{u}, \tag{7.1}$$

where $\mathbf{u}$ is the velocity vector, p is the pressure, and ∇ is the divergence operator. The above equation is often referred to as the Stokes equation, named after the mathematician Sir George Stokes. Equation (7.1) is the main equation governing the hydrodynamics of swimming microorganism and has some interesting properties. For example, the above equation is instantaneous in the sense that it has no dependence on time other than via boundary conditions. Equation (7.1) is also linear in both velocity and pressure. Furthermore, it is time-reversible in the sense that any time-reversed Stokes flow solves the same equations as the original Stokes flow. This time-reversibility, or kinematic reversibility, forms the hydrodynamic basis of the "scallop theorem" introduced earlier [1]. These properties illustrate that swimming at low Reynolds numbers can seem at first as a highly confined phenomenon, yet microorganisms have found a variety of ways to overcome the constraints of the scallop theorem. In what follows, we briefly review some of the classical theories that have shed light on the hydrodynamic mechanisms leading to net propulsion at low Reynolds numbers. The discussion will be limited but the reader can find a more thorough review in [2, 5, 8, 30] as well as in Chaps. 1 and 8 of this book.

Over half a century ago, Taylor [27, 28] beautifully demonstrated that an infinite waving sheet (see Fig. 7.2a) could swim in an incompressible, Newtonian fluid by generating traveling waves in the absence of inertia or vanishing Reynolds numbers. Note that the hydrodynamics of Taylor's waving sheet is governed by Eq. (7.1). In Taylor's work, the planar sheet oscillates in time *in a prescribed form* according to $y(x,t) = a\sin(kx - \omega t)$, where a is the traveling wave amplitude, ω is the frequency, $\lambda = 2\pi/k$ is the wavelength, $c = \omega/k$ is the traveling wave speed, and k is the wave number. Taylor found that the sheet oscillations induce a forward velocity $U = \omega a^2 k/2 + \mathcal{O}(ka)^4$ [27], where the sheet is propelled in the direction opposite to that of the propagating wave (Fig. 7.2a).

Many important investigations followed Taylor's landmark contribution. Of particular relevance, we highlight the well-known resistive force theory (RFT) introduced by Gray and Hancock in analyzing the locomotion of sperm cells [3]. There, the authors assumed that the hydrodynamic forces experienced by the

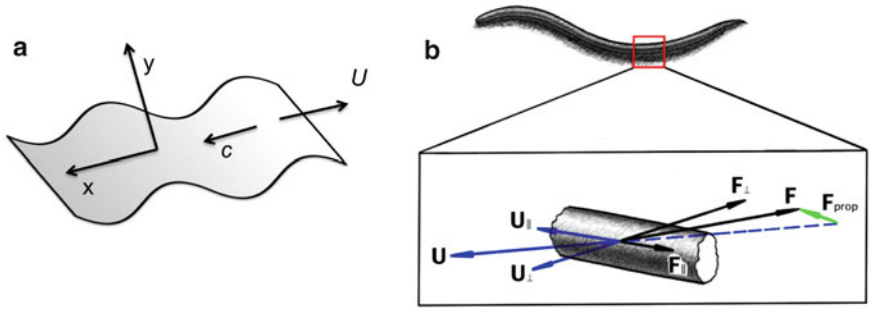

Fig. 7.2 (**a**) Two-dimensional waving sheet in a viscous fluid illustrating the traveling wave of velocity c progressing in the x-direction and the forward swimming speed (U) in opposite direction. (**b**) Resistive force theory (RFT) diagram illustrating the normal and tangential components of the velocity U and force F, and the resulting net propulsive force

organism would be approximately proportional to the local body velocity such that the force exerted by a body or flagellar segment is given by $\mathbf{F} = C_N\mathbf{U_N} + C_T\mathbf{U_T}$, where C corresponds to the local drag coefficient per unit length (dependent on geometry and fluid viscosity) and N and T are the normal and tangential components, respectively (see Fig. 7.2b). Hence, the total thrust can then be obtained by integrating the propulsive force over the entire body or flagellum length. It is namely the anisotropy between the normal and tangential drag coefficients, with $C_N > C_T$, that lies at the origin of the drag-based thrust.

Using RFT, Gray and Hancock obtained (for the case of large-amplitude displacements) a closed-form solution for the swimming speed of an undulating filament given by the expression $U = \pi c(a/\lambda)^2(C_N/C_T - 1)/\ (1 + 2\pi^2(C_N/C_T)(a/\lambda)^2)$. Here, $C_N = 2C_N = 4\pi\mu/\ln(L/a)$ for a straight rod of length L such that the ratio of normal to tangential drag coefficients yields $C_N/C_T = 2$ for a sine wave of wavelength λ where a is the amplitude. For example, more recent experiments using the nematode *C. elegans* estimated this ratio at $C_N/C_T = 1.4$ [7]; such value lies closely with earlier estimates reported by Gray and Lissmann [6] who dropped thin wires into viscous fluids ($C_N/C_T = 1.4$–1.6).

Lighthill [9] later recognized the importance of long-range hydrodynamic interactions and improved RFT by incorporating slender-body approximations. Such improvements led to $C_N/C_T = 1.5$ for the case of an undulating filament swimming in an infinite fluid medium. When incorporating wall effects into the analysis, a significantly larger value of the drag coefficient ratio ($C_N/C_T = 4.1$) was subsequently obtained using the corrections of Katz et al. [32].

But what can we say about the flow fields generated by swimming microorganisms in fluids? A common way to determine flow fields at low Reynolds numbers is to solve the Stokes equation [Eq. (7.1)] with a forcing term replaced by a point force or disturbance [33]. As noted earlier, the flow disturbances driven by the swimming motion of microorganism in a Newtonian fluid depend linearly upon the stresses exerted by the moving body on the fluid [see Eq. (7.1)]. These boundary-driven

flows are known to decay very slowly with the distance r away from the body [2, 8, 34]. Most often, such flow disturbances are mathematically cast as linear superpositions of the fundamental solutions of the Stokes equation and decay with inverse powers of r. The first solution, referred to as a "Stokeslet," arises from the net force on the fluid, and has a velocity field that decays as $1/r$. The next solution, also known as a "stresslet" flow, is induced by the first force moment exerted by the body on the fluid and decays more rapidly ($1/r^2$); higher-order solutions decay even more rapidly ($1/r^3$). As a result, linear combinations of the basic solutions of the creeping equations of fluid motion can generate a multitude of complex flow fields, exhibiting contrasting near- and far-field behaviors [34].

3 Experiments in Newtonian Fluids

Experimental studies on low Reynolds number locomotion in Newtonian fluids have undoubtedly complemented early theories on the topic [3, 4, 6, 9, 27, 28]. Many of these works have aimed at addressing the validity of classical theoretical models. In the section below, we briefly review a number of relevant experimental efforts that have helped over time characterize low Reynolds propulsion in Newtonian media.

3.1 From Scale-Up Models to Live Microorganisms

Scale-Up Experiments Experiments with live microorganisms are generally challenging due to difficulties with imaging/optical setups and to the lack of control over the organisms themselves. One attractive experimental approach to circumvent some of these issues relies on leveraging scale-up systems, often designed to mimic the organism's main swimming kinematics (see Fig. 7.3). Scale-up models provide much valuable insight into the main physical mechanisms governing micro-swimming phenomena; they have brought valuable insight in understanding the net motion resulting from traveling waves along elastic tails [35–37], helical flagella [38, 39], and flagellar bundles [40, 41] as well as in uncovering the motility resulting from surface traveling waves along cylindrical shells [42].

Beyond fundamental research into microorganism locomotion, a broad range of scale-up designs has been employed in the context of artificial swimming strategies at low Reynolds numbers [8], including Purcell's seminal "three-link swimmer" which possesses two hinges actuated with both time and phase differences [43] and a flapping body performing reciprocal motions near a deformable free surface [44]. Smaller mechanical systems have also been investigated. For example, the shapes of an oscillating passive actin filament have been experimentally probed [45] and more recently, a three-sphere design has been implemented using colloidal beads and optical tweezers [46]. There is also much interest in artificial micro-swimmers from the robotics and engineering community [47].

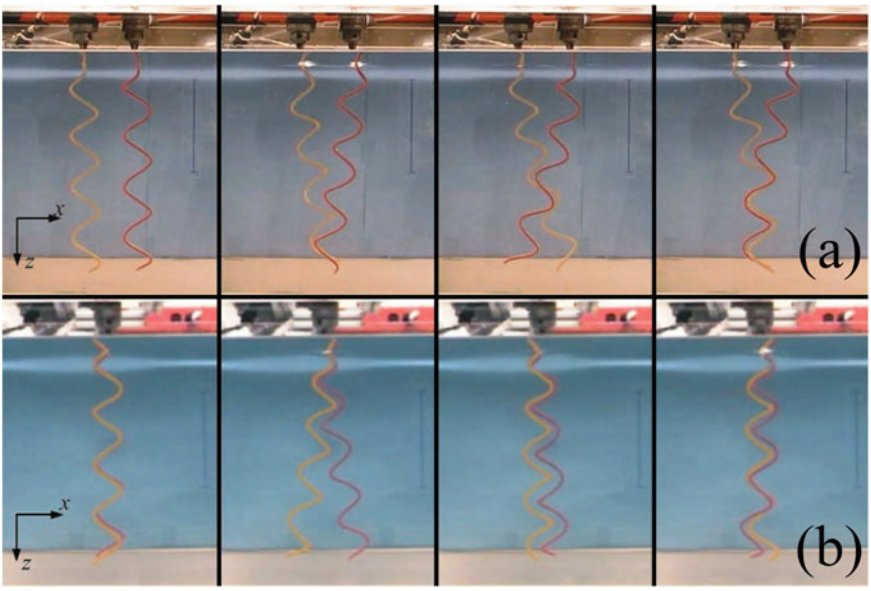

Fig. 7.3 Example of scale-up model of flagellar bundling dynamics [40]. (**a**) Image sequence of semi-coiled helices shown at various instances in time. (**b**) Same helices viewed from the side. The scale bars are 100 mm long; the helices are 310 mm long (from chuck to tip), 4.0 mm in diameter, and turning at 0.1 Hz ($\mathrm{Re}_{\mathrm{freq}} \approx 3 \times 10^{-5}$). Copyright (2003) National Academy of Sciences, USA

Experiments with Live Microorganisms Despite challenges in working with live microorganisms, microscopy imaging of bacterial flagella has gained tremendous traction following the pioneering work of Berg [13,14,48–50]. Of utmost relevance, flagellar kinematics of individual bacteria have been visualized in real time using fluorescent staining of both cells and flagellar filaments [51]. In more recent years, these initial microscopy techniques have been further developed to obtain time-resolved imaging of flagellar motility using setups with high-speed cameras [52] as well as to track swimming microorganisms three-dimensionally (3D), for instance, in a fluid far from surfaces [53]. These exquisite measurements provide much valuable data for our understanding of swimming and for the development of more realistic models.

Since, however, microorganisms evolve constantly near solid boundaries (e.g., migration of infectious bacteria through tissues), a growing number of experiments have shown that it is important to consider the presence of surfaces; namely, surfaces and wall effects drastically alter the kinematics of swimming microorganisms relative to ideal unbounded swimming conditions. A best-known example is perhaps illustrated for helical flagella (e.g., *E. coli*): swimming trajectories are modified from straight to circular in the vicinity of boundaries, clockwise when the wall is rigid [54] and anticlockwise near a free surface [55]. In particular, solid surfaces not only lead to the reorientation of microorganisms in the direction parallel to the surfaces, they also attract the organism to the closest wall [56].

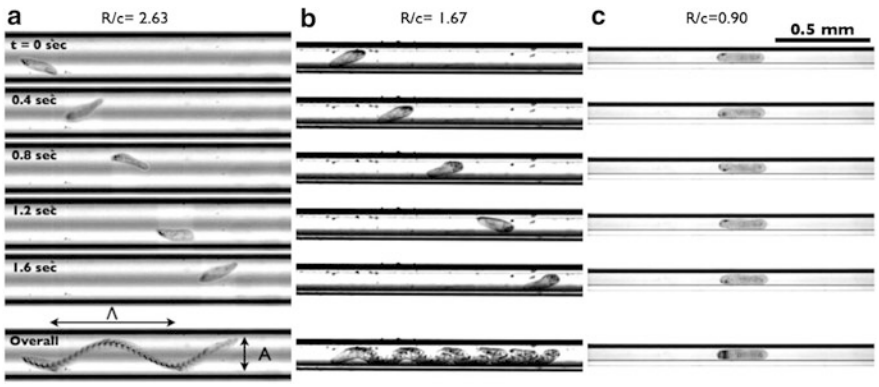

Fig. 7.4 Swimming of *Paramecium* in tubes of different diameters [60]. Here, Λ denotes the wavelength, c denotes the radius of the organism, and A the amplitude of the helical trajectory traced by the organism in tubes of different diameter. **(a)** *Paramecium* swimming in large tube ($R/c = 2.63$) where the trajectory of the motion is helical. **(b)** Small wavelength helices are seen inside tubes of intermediate diameters ($R/c = 1.67$). **(c)** In very small tubes ($R/c = 0.9$), *Paramecium* swims in a *straight line*. Figure reproduced with permission from the American Institute of Physics

Uncovering the fundamental hydrodynamic interactions between surfaces and swimming microorganisms has helped shed light on experimental observations of the accumulation of confined spermatozoa on boundaries [57–59]. It was recently observed [60] that ciliated *Paramecium* swimming in capillary tubes executes helical trajectories that slowly transition to straight lines as the tube diameter decreases (Fig. 7.4). Further experimental studies mimicking bio-locomotion in confined environments (e.g., female reproductive tract) have also revealed that the migration of motile spermatozoa in 3D microchannels is strongly influenced by specific wall shapes, including the turning angles at corners [61]. Beyond single-cell eukaryotic and prokaryotic microorganisms, it has also been noted that multicellular organisms, such as *C. elegans*, may display some finite attraction to the presence of boundaries [62] and certainly exhibit changes in their swimming kinematics under confinement conditions (e.g., setups with parallel-wall cells) [63]. As we can see, the presence of surfaces, solid or fluid-like, can significantly affect the dynamics of swimming microorganisms and cannot be ignored.

3.2 Propulsive Force and Flow Measurements

There has also been much effort in measuring the propulsive forces (i.e., thrust) and energy generated by swimming microorganisms. For instance, optical traps have been used to measure the forces required to tether sperm cells and bacteria [31, 64, 65]. In parallel, atomic force microscopy (AFM) has enabled the measurements of forces exerted by mucus-propelling cilia that lie on the order of

< 1 nN per cilium during the effective stroke [66]. Recently, force measurements using optical tweezers have been obtained on individual bacteria to test the validity of RFT and determine the swimming efficiency of *E. coli* [67]. These latter measurements have revealed for the first time that long-range hydrodynamic interactions are indeed critical in capturing accurately single-cell propulsion; in contrast, relying on RFT assumes a stationary background fluid while ignoring local flows induced from the other moving parts of the cell. Such observations have been most recently corroborated in scale-up models of helical flagella, where the validity of RFT breaks down for increasing pitch angles of the helix [39].

Concurrently, macroscopic (scale-up) experiments with helical bodies of different wavelengths λ, radii R, and lengths L (relevant to bacterial flagella) have highlighted the qualitative and quantitative discrepancies with RFT predictions [68]. This may be ascribed to the fact that RFT only takes into account local effects and neglects any hydrodynamic interactions between different parts of the swimmer. More accurate results can be obtained by using slender-body theories (SBT) that exploit the high aspect ratios seen in swimmer geometries and are based on the use of singularity solutions to the Stokes equations [69–72]. Since nonlocal hydrodynamic interactions between different parts of the swimmer may be incorporated in these theories, they provide much better results. While analytical expressions for the drag forces are generally difficult to obtain (here RFT can be of much value [9]), numerical solutions have been used to choose between different forms of resistance coefficients [73, 74] as well as study swimming in eukaryotic swimmers [75].

Despite the tremendous experimental progress, it is still difficult to measure the flow fields generated by swimming microorganisms due to limited spatial resolution of common velocimetry methods. One of the first attempts of visualizing the flow of swimming organism dates back to the1960s when Gray and Lissmann [6] presented qualitative path lines of freely swimming nematodes (worms) in water seeded with starch grains. With the advent of modern micro-PIV (μPIV) techniques [76] and fast cameras, flow field measurements of swimming microorganisms are within reach. For example, path lines generated by an individual ciliated *Paramecium* have been recently imaged [60], and velocity fields generated by individual unicellular microorganisms [52] and multicellular nematodes [7] have been resolved. In the case of the swimming nematode [7], the authors demonstrated that velocity magnitudes of fluid motion follow closely an exponential decay of the form $\exp(-2\pi r/\lambda)$ as a function of the distance r away from the nematode body (see Fig. 7.5); this analytical solution was originally derived by Lighthill [9] for an undulating sheet of wavelength λ in Stokes flow. Further extension of high-speed imaging techniques using for example tomographic PIV, where multiple cameras image simultaneously the interrogation volume from different angles [77], has enabled measurements of 3D time-resolved flow fields surrounding millimeter-sized copepods (*Calanus finmarchicus*).

There are two recent experiments [78, 79] that deserve much consideration and attention. The experiments by Drescher et al. [78] and Guasto et al. [79] were able

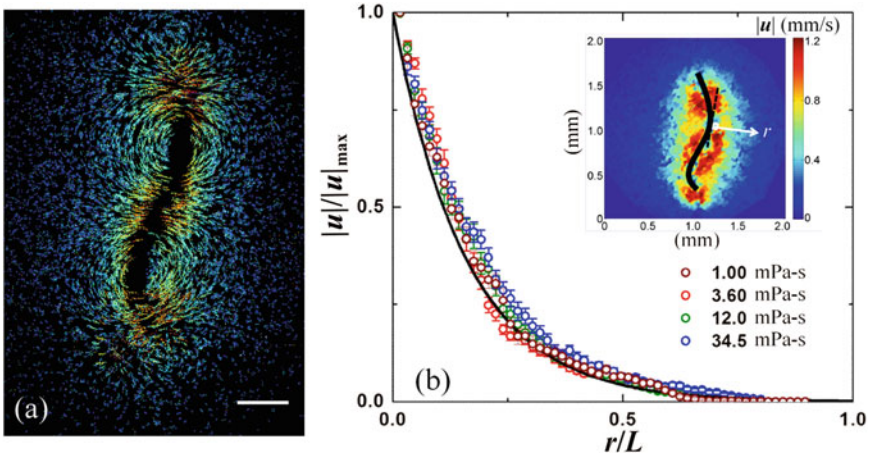

Fig. 7.5 Flow behavior surrounding a swimming *C. elegans*. Adapted from Sznitman et al. [7]. **(a)** Color-coded particle path lines are shown via the trace of dispersed fluorescent particles. Particle trajectories are tracked over ten consecutive frames (~ 0.06 s). Colors are associated with the lengths of trajectories. Two dominant recirculation regions are resolved along the nematode body. Scale bar represents 200 µm. **(b)** Normalized fluid velocity magnitude ($|\mathbf{u}|/|\mathbf{u}|_{\max}$) as a function of the dimensionless distance (r/L) away from the nematode body, where L is the nematode body length. Data points of different colors correspond to fluids of different viscosities. The *solid line* corresponds to $\exp(-2\pi r/\lambda)$ [9]. *Inset*: representative velocity magnitude field at a given instant in time surrounding a nematode (marked with a *black line*). Figure reproduced with permission from the American Institute of Physics

to beautifully resolve the flow fields surrounding freely swimming micro-algae and demonstrated that local fluid motions were much more complex than analytical models initially suggested. This observation is particularly true in the near field, where the largest flow velocities occur. For example, Drescher et al. detailed quantitative measurements of time-averaged flows using μPIV for two different types of microalgae: *Volvox carteri*, a ciliated multicellular spherical alga, and *Chlamydomonas reinhardtii*, a unicellular alga featuring two flagella that beat in a breaststroke-like fashion. Guasto et al. resolved rather the oscillatory nature of the flow field driven by *C. reinhardtii* over one period of motion using high-speed imaging, where the swimming microorganisms were confined in thin liquid films. Both studies have emphasized how distinct species are likely to drive qualitatively different disturbance flows, as recently highlighted by Saintillan [34]. This flow feature remains true in the far field as well, where it is commonly assumed that there, flow fields can be described in terms of a stresslet. As a final word, we note that the representation of these driven flows using time-averaged velocity fields falls short of capturing the true nature of the flow, since time fluctuations can be of the same order as the mean.

4 From Newtonian to Complex Fluids

As mentioned before, much of our understanding of low Reynolds number locomotion arises from considerations in simple, Newtonian fluids [2–4, 9]. Many microorganisms, however, evolve and live in complex fluids such as mucus, gels, and wet soil [80–83]. But, what are complex fluids? Here, we define complex fluids as a broad class of materials that are usually homogeneous at the macroscopic scale and disordered at the microscopic scale, but possess structure at an intermediate scale (typically, a few sizes of its particles). Examples include colloidal suspensions, foams and emulsions, polymeric fluids, gels, human mucus, and blood. In colloidal crystals, for example, the intermediate scale is set by the size of the organized crystalline structure; that is, if one considers a cup of a cornstarch suspension, then the microscopic scale is the matrix that includes both the water molecules and the cornstarch grains ($\sim 1\,\mu$m), and the macroscopic scale is the size of the cup ($\sim 10\,$cm), while the intermediate scale is set by the structural length scale (if any) of the cornstarch grains. The cornstarch suspension will respond quite differently to an applied stress, depending on the grain size, concentration, and the grain arrangement in the suspending liquid. Thus, the macroscopic flow behavior (or rheology) of complex fluids is a strong function of the fluid microstructure.

Complex fluids are usually not Newtonian, and they often exhibit viscoelasticity and shear-thinning viscosity. Much recent effort has been devoted to the understanding of the effects of non-Newtonian fluid behavior (shear-thinning, viscoelasticity) on the swimming of microorganisms [8, 80, 81, 83, 84]. For example, the nonlinear relationship between shear stress and strain rate that characterizes shear-thinning fluids can have significant consequences to locomotion at low Reynolds numbers including (i) a breakdown of the "scallop" theorem, (ii) kinematic changes in the organism's swimming motion, and (iii) changes in the drag forces experienced by the organism. In fact, it was recently shown by Vélez-Cordero and Lauga [85] for an infinite waving sheet (similar to Taylor's original work) immersed in a shear-thinning fluid that while the sheet's propulsion speed remained the same as in the Newtonian case, the cost of transport was reduced. Simulation studies by Montenegro-Johnson et al. [84] showed that undulatory swimmers with a head or "payload" (similar to a sperm cell) are assisted by shear-thinning viscosity, resulting in increased speed. These recent studies illustrate that even relatively simple non-Newtonian fluid behavior such as shear-thinning may have a significant impact on the swimming behavior of microorganisms.

The effects of fluid elasticity on swimming at low Reynolds numbers have received considerable more attention [83, 86–93] than shear-thinning effects. Viscoelastic fluids possess shear stress that is time dependent and that depends on the history of deformation. Such features give rise to flow behavior in viscoelastic fluids that is markedly different from that of Newtonian fluids even at low Reynolds numbers [94–96], and they can even lead to the breakdown of the scallop theorem [92]. Most of the nonlinear flow behavior observed in the flow of viscoelastic fluids results from the extra elastic stresses due to the presence, of

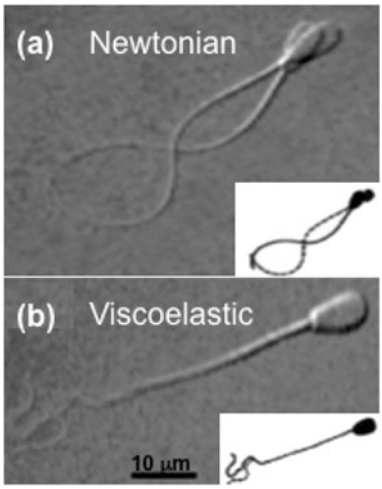

Fig. 7.6 Snapshot of sperm cells moving in (**a**) Newtonian fluid (semen) and viscoelastic fluid (mucus); adapted from Ho and Suarez [97]

usually, polymer molecules in the fluid. Mechanical stresses in viscoelastic fluids are history-dependent and depend namely on a characteristic time λ that in dilute solutions is proportional to the relaxation time of a single polymer molecule. In semi-dilute solutions, λ depends also on molecular interactions. For more details on fluid viscoelasticity and shear-thinning viscosity, please see Chaps. 1, 8, and 10.

The nonlinear response of viscoelastic fluids is expected and has been seen to play a significant role on the swimming behavior of microorganisms. Consider for example the swimming behavior of motile sperm cells [86, 97, 98] that usually swim as a result of (single) flagellar beating. For freely swimming spermatozoa in Newtonian semen (Fig. 7.6a), the flagellum exhibits a regular sinusoidal beating pattern [81]. But once the organism encounters a viscoelastic medium (i.e., cervical mucus), the regular beating pattern is transformed into high-amplitude, asymmetric bending of the flagellum (Fig. 7.6b). This "hyper-activated" sperm is believed to be dramatically influenced by its fluidic environment [81, 97], which in turn can affect human fertility [80, 99]. Other examples of motility in viscoelastic media include the removal of mucus in the human respiratory track by beating cilia [24, 26], the locomotion of bacteria in biofilms [100, 101], and the burrowing of organisms in wet soil [102, 103]. Understanding how microorganisms move in viscoelastic fluids is, therefore, of both scientific and practical importance.

Despite many recent efforts to be discussed below, the effects of bulk fluid elasticity on the motility behavior of live organisms at low Reynolds numbers are still not clear and well understood. In order to provide the reader with some basic insight into this issue, we turn to our favorite dimensionless parameters. The first, of course, is the Reynolds number, which is a measure of the relative importance of the fluid inertia to viscous forces. We already showed that the Reynolds number is approximately 10^{-4} for *E. coli* swimming in water. The effects of fluid elasticity are often estimated using the Deborah number, defined as $\mathrm{De} = \lambda f$ where λ is the fluid relaxation time and f is the organism's beating frequency. Note that $\mathrm{De} = 0$ for

Newtonian fluids and De $\to \infty$ for purely elastic solids. One could imagine that fluid elasticity may begin to play a dominant role for De ≥ 1. If one considers the beating frequency f of sperm cells to range from 20 to 50 Hz and the relaxation time λ of cervical mucus to range from 1 to 10 s (depending on factors like hydration, among others), one can expect fluid elasticity to play a significant role on the motility of spermatozoa since De $\gg 1$. One can also compare the ratio of the (fluid) elastic time scale λ to the (fluid) viscous time scale $\rho L^2/\mu$. This is the so-called elasticity number, defined as $\mathrm{El} = \lambda\mu/\rho L^2$. Elastic effects are expected to dominate for El > 1. Because of the nonlinear (squared) dependence of El on the (swimmer) length scale L, one anticipates the effects of fluid elasticity to become increasingly important for swimming microorganisms.

4.1 Swimming in Viscoelastic Fluids: Expectations

In 1979, Chaudhury [87] attempted to incorporate the effects of fluid elasticity on swimming using a second-order fluid and a series of expansions similar to Taylor's analysis. It was then predicted that fluid elasticity could either increase or decrease the propulsion speed of the waving sheet (Fig. 7.2), depending on the value of Re. Later, inspired by experimental observations of spermatozoa swimming in mucus [81, 97], the effects of elasticity on beating flagellar structures were considered in Stokes flow using the Maxwell model [104]. It was shown that self-propulsion was not affected by viscoelasticity even at large Deborah numbers (De), where De $= \lambda f$ and λ is the fluid relaxation time and f is the beating frequency. However, the total work decreased with increasing De. It was then suggested that a microorganism could swim faster in a viscoelastic fluid with the same expenditure of energy compared with a Newtonian fluid.

More recently, Lauga [83] showed that, for a 2D waving sheet (Fig. 7.2), elastic stresses could significantly alter the organism speed and the work required to achieve net motion. Using nonlinear viscoelastic fluid models such as the Oldroyd-B and the FENE-P models (see Chap. 1), Lauga [83] showed that the sheet's forward speed U in a purely elastic fluids is given by

$$\frac{U}{U_N} = \frac{1 + \mathrm{De}^2(\eta_s/\eta)}{1 + \mathrm{De}^2}, \tag{7.2}$$

where U_N is the swimming speed of the sheet in a viscous Newtonian fluid (i.e., Taylor's original result) and η_s is the solvent viscosity; note that the solution viscosity η is assumed to be the sum of the solvent viscosity and the polymer viscosity such that $\eta = \eta_s + \eta_p$. Hence, for a given (i.e., prescribed) swimming gait $U_N \geq U$, that is, elastic stresses reduce the overall speed of the waving sheet. Equation (7.2) is an elegant and interesting result and has spurred much of the recent interest in swimming in viscoelastic fluids. See Chap. 8 for a more detailed discussion on the derivation of Eq. (7.2).

A similar result to Eq. (7.2) was also obtained for a waving cylinder by Fu et al. [88]. These important results imply that fluid elasticity can reduce the swimming speed of microorganisms when compared to simple, Newtonian fluids. An important caveat, of course, is that organisms may compensate the reduction in velocity by increasing their beating frequency and/or concurrently decreasing their body wavelength. In other words, microorganisms can alter their swimming kinematics to adjust or adapt to varying fluidic environments. It is worth noting that the analysis by Lauga [83] and Fu et al. [88] reveals the net magnitude of locomotion scales quadratically with the amplitude of the local oscillatory motion, and therefore nonlinear terms in viscoelastic constitutive relationships cannot be neglected (as in the case of [104]).

Numerical simulations have also been used to address the role of fluid elasticity on the swimming behavior of microorganisms. In particular, Teran and co-workers [89] considered two-dimensional swimming "free" sheets (i.e., with free head and tail) of *finite* length L in viscoelastic fluids. The simulations were performed by solving Stokes equation using the Oldroyd-B model as the constitutive equation using an immersed boundary method. The simulations show that, for accentuated tail motions, the sheet swims faster at De ≈ 1 than in a Newtonian fluid. This regime corresponds to where "swimmer" stroke frequency matches the fluid relaxation time. This is a fascinating result and is unlike Eq. (7.2) which predicts that the swimmer speed in viscoelastic fluids is always slower than in Newtonian fluids. The simulations do show that for De > 1, the swimming speed decreases as De increases (Fig. 7.7).

As briefly discussed above, fluid elasticity can strongly affect both the swimming dynamics and kinematics of microorganisms even at low Reynolds numbers. Recent analytical works predict that fluid elasticity hinders swimming speed while numerical simulations show that it is possible to obtain an enhancement in self-propulsion

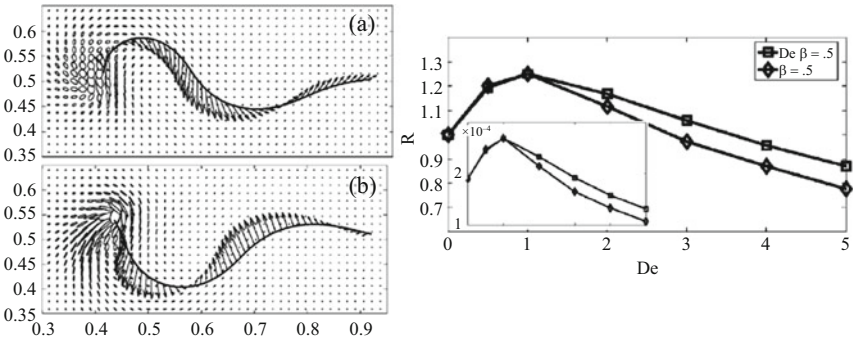

Fig. 7.7 (**a,b**) Polymer stress tensor fields for a finite length, two-dimensional undulating sheet. The *ellipses* in the figures represent the directions and degree of distension of the polymer field. The *arrows* represent the fluid velocity on the immersed filament. (**c**) Normalized average swimming speed of the sheet as a function of the Deborah number. Note the enhancement in propulsion at De ≈ 1. Figures adapted from [89]

in a regime where the fluid relaxation time matches the swimmer stroke frequency, that is De ≈ 1. Despite such important advances, it is still not clear whether elastic stresses enhance or hamper self-propulsion since theoretical and numerical results are model dependent. So the question still stands: does fluid elasticity enhance or hinder self-propulsion at low Re? Perhaps experiments will shed more light into this important question.

5 Experiments in Viscoelastic Fluids

5.1 Scale-Up Experiments

Swimming experiments in complex fluids are hard to come by and *systematic* investigations are scarce in the literature. Part of the problem is undoubtedly the difficulty in identifying a model organism or swimmer that is both able to move in different types of media and relatively easy to image and track. To circumvent some of these difficulties, many investigators choose to build instead macroscopic-scaled versions of the microorganisms' propulsion mechanism [35, 41, 90, 105]. In this section, we discuss an interesting experimental setup proposed by Liu and coworkers [90] in which a scale-up model of bacterial filaments is investigated.

The experimental setup is shown in Fig. 7.8 and consists of a large cylindrical tank filled with either a viscous Newtonian fluid or a viscoelastic fluid. The Newtonian fluid is silicon oil and the polymeric solution is a mixture of polyisobutylene

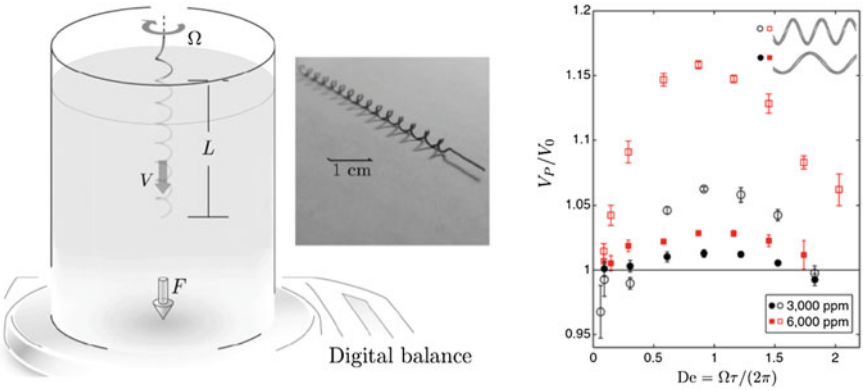

Fig. 7.8 (**a**) Scale-up mechanical apparatus used for measuring the motility of a rotating helix [90]. The helical structure, shown in (**b**), is slowly immersed into a Newtonian or viscoelastic fluid and rotates about the vertical direction. The net hydrodynamic force on the helix is determined by a laboratory balance beneath the tank as shown in (**a**). (**c**) Normalized propulsion speed as a function of the Deborah number for two polymeric solutions and helices with different pitch angles. Copyright (2011) National Academy of Sciences, USA

(PIB) in polybutene solvent. More details on the polymeric solutions are given in the next paragraph and in [90]. A rigid helix rotating at speed ω is slowly immersed or plunged at a constant speed into fluid-filled tank. Helices of varying pitch angles are used to mimic the geometry of bacterial flagellar filaments (e.g., *E. coli*). The hydrodynamic force exerted on the helices by the fluid is measured by placing the tank on top of a sensitive digital balance. In these experiments, zero-force swimming is achieved by adjusting the translation speed until the measured axial force is zero. Because the helix is inserted from above, a positive vertical force on the helix represents a drag, and a negative vertical force on the helix is a thrust. The force-free swimming speed is measured as a function of helix rotation rate, helix geometry (i.e., pitch angle), and fluid properties (i.e., Newtonian vs. viscoelastic).

Because the fluids are very viscous, the Reynolds number is well below 0.01 and inertial effects are negligible. In order to decouple the effects of fluid elasticity from those of rate-dependent viscosity (e.g., shear-thinning) common in polymeric solutions, a nearly constant-viscosity, elastic fluid was prepared. Such fluids are often called "Boger fluids" in reference to David Boger who first proposed the use of such model fluids [106]. Boger fluids are constructed by adding a small amount (usually in part per millions) of high molecular weight (MW) flexible polymer to a very viscous solvent. Because the polymer contribution to the overall solution viscosity is small, the solution viscosity is overwhelmed by the viscosity of the Newtonian solvent. But the addition of high MW flexible polymers is able to add elasticity to the fluids. As a result, Boger fluids have nearly constant viscosity while still possessing elasticity. In the work of Liu et al. [90], Boger fluids are prepared by dissolving either 3,000 ppm or 6,000 ppm of PIB in polybutene (solvent). The average relaxation time λ for both polymeric solutions is approximately 0.6 s.

The main result of this very clever experiment is shown in Fig. 7.8 (rightmost panel). The investigators find an enhancement of the measured swimming speed of a rotating helix in a viscoelastic fluid near $\mathrm{De} = 1$, where $\mathrm{De} = \omega\lambda/2\pi$. This result is similar to the enhancement observed in numerical simulations of 2D flexible filaments in Oldroyd-B fluids by Teran and coworkers [89] and of helical filaments [93], but is in contrast with the decrease observed in analytical calculations [83, 107] and experiments with live organisms [91]. As the rotating speed (and De) increases, the helix propulsion speed decreases even below the purely viscous Newtonian speed.

An important take-away message is that it appears that the nature of the dependence of propulsion speed on fluid elasticity (or De) depends strongly on the geometry of the waveform used for swimming. This is made obvious by the sensitivity of the peak enhancement of swimming speed on the pitch angle of the helix, as shown in Fig. 7.8 (rightmost panel). This is an important point which we will further discuss later in this chapter.

While scale-up experiments can provide much useful information, they cannot fully capture the complexity of live organisms. Therefore, it is important to perform systematic studies using live organisms. In the next section, we will discuss experiments using a well-known biological model system, namely, the nematode *C. elegans*.

5.2 *Experiments with Live Organisms*

Despite recent advances, the effects of fluid elasticity on the swimming behavior of microorganisms are still not clear [108], in part due to the lack of systematic experiments with live organisms. In this section, we will discuss swimming experiments in viscoelastic fluids with a biological model system, namely the nematode *C. elegans*. Model organisms are nonhuman species which are extensively studied to understand particular biological phenomena. Examples include the zebra fish, *E. coli*, fruit fly (*Drosophila melanogaster*), and mice, among many others. The idea is that discoveries made in model organisms will provide insight into the workings of other non-model organisms.

5.2.1 *C. elegans*: An Attractive Model Organism for Swimming Studies

An interesting model system that has received much attention in the biological community is nematode *C. elegans*, which is a small, multicellular, free-living roundworm found in soil environments. Much is known about the nematode's genetics and physiology; its genome has been completely sequenced [109] and a complete cell lineage has been established [110]. These nematodes are equipped with 95 muscle cells that are highly similar in both anatomy and molecular makeup to vertebrate skeletal muscle [11]. Their neuromuscular system controls their body undulations which allows *C. elegans* to swim, dig, and crawl through diverse environments. The wealth of biological knowledge accumulated to date makes *C. elegans* ideal candidates for investigations that combine aspects of biology, biomechanics, and the fluid mechanics of propulsion.

Figure 7.9 shows an image of an adult, wild-type *C. elegans* swimming in a water-like buffer (M9) solution. The nematode is characterized by a relatively long and quasi-cylindrical body shape (Fig. 7.9). Its length can vary from 50 µm (embryonic stage) to 1 mm (adult stage) while its radius is approximately 80 µm. The nematode length scale is an important feature they are large enough that flow fields can be accurately obtained.

5.2.2 Swimming Experiments with *C. elegans*: Dilute Polymeric Solutions

We now discuss swimming experiments using the nematode *C. elegans* in some detail. Experiments with the two main types of fluids, namely Newtonian and viscoelastic, are discussed. Experiments are performed in small channels that are made of acrylic and are 1.5 mm wide and 500 µm deep; they are sealed with a thin (0.13 mm) cover glass. In order to minimize three-dimensional motion, the channels are relatively shallow, yet the nematode is able to freely move in all directions. The swimming motion of *C. elegans* is imaged using standard bright-field microscopy and a fast CMOS camera. The image acquisition rate is kept constant at 125

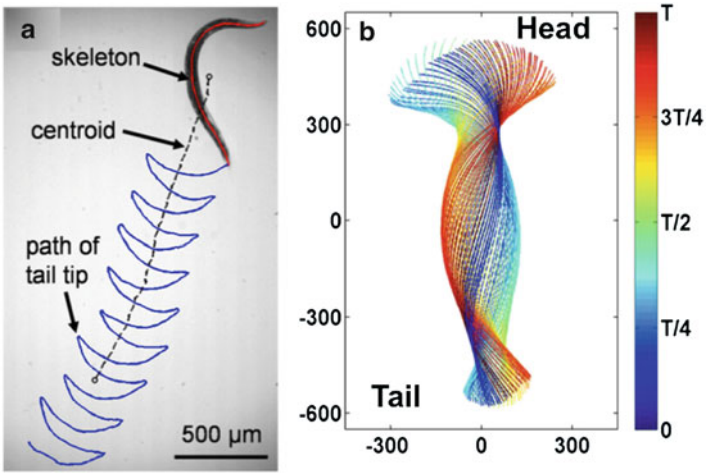

Fig. 7.9 (**a**) Snapshot of the nematode *C. elegans* moving in a water-like buffer solution. The *red line* along the nematode corresponds to the body centerline or "skeleton," obtained using image analysis. The centroid (*dashed*) and the trajectory of the tail (*blue*) are tracked at a sampling rate of 125 frames per second. (b) *Body-shape lines* as a function of time color-coded by time over one beating period

frames per second to guarantee small linear displacements along the nematode's body between consecutive frames. All data presented here pertain to nematodes swimming at the center plane of the fluidic channel. Out-of-plane recordings are discarded.

An important consideration in swimming experiments with live organisms is the fluid medium. Fluids must be developed such that they possess the desirable rheological property (elasticity, shear-thinning, etc.) but without being toxic to the organism. Here, Newtonian fluids of different shear viscosities are prepared by mixing two low molecular weight oils (halocarbon oil, Sigma-Aldrich). Viscoelastic fluids are prepared by adding small amounts of carboxymethyl cellulose (CMC, 7×10^5 MW) into deionized water. CMC is a long, flexible polymer with an overlap concentration (c^*) of approximately 10^4 ppm. In order to rule out the effects of shear-rate-dependent viscosity, an aqueous solution of the stiff polymer xanthan gum (XG) that is shear-thinning but possesses negligible elasticity is also used in experiments.

Fluid Rheology: Viscosity Data An important step in these experiments is fluid rheological characterization. How viscous or elastic are the fluids? (A very useful discussion on fluid characterization and rheology is given in Chap. 6.) A strain-controlled rheometer RSF III (TA Instruments) with a cone-and-plate geometry is used to characterize the rheological properties of the CMC and XG solutions. Figure 7.10 shows the viscosity curves of both CMC and XG solutions. The viscosity data are fitted with the power-law fluid model of the type $\eta = m(\dot{\gamma})^{n-1}$,

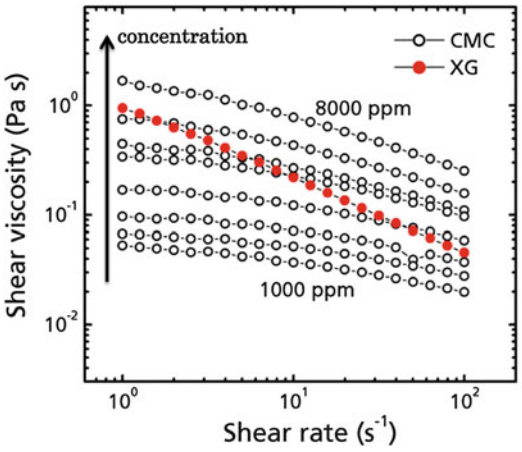

c (ppm)	n
1500	0.83
2000	0.81
3000	0.80
4500	0.76
5000	0.74
6000	0.70
8000	0.65

Fig. 7.10 (*Left*) Fluid shear viscosity curves for the flexible carboxymethyl cellulose (CMC) and semi-rigid xanthan gum (XG) solutions. The concentrations of CMC solution ranges from 1,000 ppm to 8,000 ppm by weight, from *bottom* to *top* in the plot. *Solid circles* represent the 3,000 ppm XG aqueous solution. The values of the power law index n are 0.65 and 0.35 for the 8,000 ppm CMC and the 3,000 ppm XG solutions, respectively. Table: the power law indexes of the CMC aqueous solutions

where m is a flow consistency factor and n is the power law index. Results from the fits are shown in the table in Fig. 7.10. The CMC solutions show a relatively weak shear-thinning behavior, particularly in the shear rate range of 1–20 s^{-1}. This is the range of shear rates produced by the swimming *C. elegans* in fluids. As the CMC concentration in solution increases, shear-thinning effects also increases. In the most concentrated CMC solution, i.e., at 8,000 ppm, the power law index n is approximately 0.65. As a comparison, the xanthan gum solution at 3,000 ppm shows much stronger shear-thinning behavior ($n = 0.35$). Note that the mixture of low molecular weight halocarbon oils shows constant shear viscosity and is not shown.

Fluid Rheology: Relaxation Times Shear viscosity or flow curves are not sufficient to describe the material properties of viscoelastic fluids. An important quantity used to characterize viscoelastic fluids is the fluid relaxation time λ. Measuring λ is not a trivial task for several reasons including the fact that most real viscoelastic fluids have not one but a spectrum of relaxation times; λ can also be shear rate dependent. What is usually reported in the literature (and used in many models) is the longest, most dominant value of λ. There are several ways to obtain λ including (i) measurements of the first normal stress difference N_1 from steady rheology combined with an appropriate constitutive model, (ii) oscillatory or frequency-dependent measurements in which both the viscous G'' and elastic G' moduli are measured for small strains, and (iii) stress relaxation experiments. For more detailed information on rheological measurements and applications, please see Chap. 6.

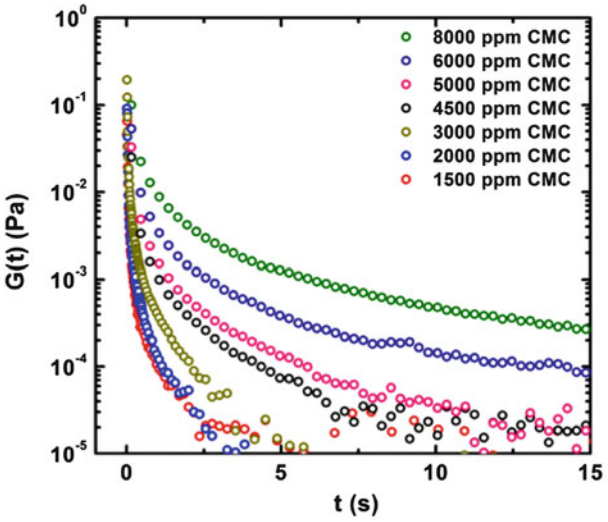

c (ppm)	λ (s)
1500	0.4
2000	0.6
3000	0.8
4500	2.1
5000	2.3
6000	3.4
8000	5.6

Fig. 7.11 (*Left*) Stress relaxation data and (table) fluid relaxation time λ for all polymeric (CMC) solutions

The values of λ for all the viscoelastic CMC solutions are obtained using a stress relaxation technique after a sudden applied strain or shearing displacement. This technique is sometimes referred to as step-strain stress relaxation. In the experiment, the time decay of the shear stress is described by a relaxation modulus $G(t)$ (Fig. 7.11), which is fitted with the generalized linear viscoelastic model of a single relaxation time of the type $G(t) = G_o e^{-t/\lambda}$. By varying the polymer concentration in solution, the values of λ can range by as much as an order of magnitude from 0.4 s for the most dilute concentration (1,500 ppm) to about 5.6 s for the most concentrated solution (8,000 ppm). The values of λ for all CMC solutions are shown in the table in Fig. 7.11.

Swimming Kinematics Now that the fluids have been characterized, we can begin to discuss the swimming experiments using *C. elegans*. Because it is important to establish a baseline, results obtained with the viscoelastic fluids (CMC solutions) are compared to swimming in Newtonian fluids (halocarbon oils). An important quantity that is used to characterize the swimming behavior of undulatory swimmers such as the nematode *C. elegans* is the bending curvature, defined as $\kappa(s,t) = d\phi/ds$=. Here, ϕ is the angle made by the tangent to the x-axis in the laboratory frame at each point along the body centerline, and s is the arc length coordinate spanning the head of the nematode ($s = 0$) to its tail ($s = L$). Note that the y-axis corresponds to the dimensionless position s/L along the nematode's body where $s = 0$ is the head and $s = L$ the tail and the x-axis cuts across the nematode as shown in Fig. 7.12a. The spatiotemporal evolution of the nematode's body curvature $\kappa(s,t)$ for 3T, or 3 swimming cycles is shown in Fig. 7.12a. The contour plots show the existence of periodic, well-defined diagonally oriented lines characteristic of

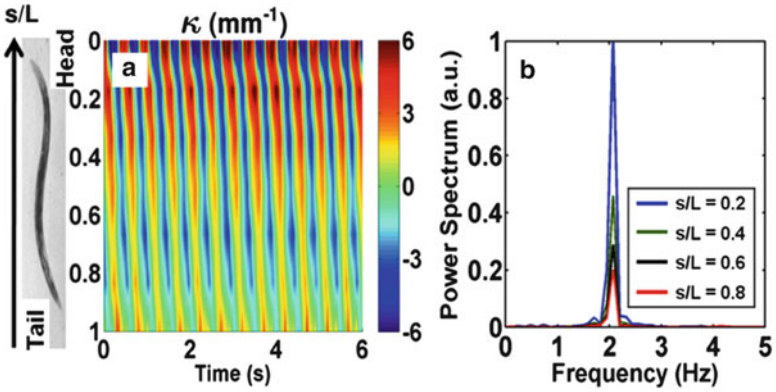

Fig. 7.12 The kinematics of swimming *C. elegans* at low Re number in viscous Newtonian fluids (Re ≈ 0.1). (**a**) Contour plot of the measured curvature (κ) along the nematode's "skeleton" or body centerlines as a function of time. The y-axis corresponds to the dimensionless position s/L along the nematode's body where $s = 0$ is the head and $s = L$ the tail; the x-axis cuts across the nematode. (**b**) Frequency spectra of κ at different selected positions s/L. The nematode's beating frequency peaks at a single value (2.0 Hz), irrespective of the location s/L

bending waves, which propagate in time along the nematode body length. By taking the Fourier transform of the contour plots (along the axis of time), a single peak at 2 Hz is found, indicating that the nematode beating is periodic in time (Fig. 7.12b). Other kinematic metrics such as wavelength (1 mm) and wave speed (5 mm/s) can also be extracted from the contour plots.

Propulsion Speed—Newtonian vs. Viscoelastic Now, it is possible to address the question of whether fluid elasticity hinders or enhances the propulsion speed of live organisms using *C. elegans*. The average nematode forward velocity U is calculated by differentiating the nematode's centroid position with respect to time (Fig. 7.9). For nematodes swimming in a Newtonian fluid of shear viscosity μ of 5 mPa · s (or 5× the viscosity of water), the value of U is approximately 0.4 mm/s and the Reynolds number (Re $= \rho UL/\mu$) is approximately 0.05. Hence, the model organism *C. elegans* can be considered a low Re swimmer.

The nematode's swimming speed as a function of fluid viscosity for both Newtonian and viscoelastic (CMC) solutions is shown in Fig. 7.13a. For relatively low viscosity values, the swimming speed is independent of fluid viscosity μ and the values of U are nearly identical for both cases. For $\mu > 30$ mPa · s, the swimming speed decreases with increasing μ even for Newtonian fluids. This decrease in U is most likely due to the nematode's finite power. Note that, for a nematode swimming with constant power at low Re, $P \sim \mu U^2$ where P is power. Results show that, over the admittedly limited range of μ, the nematode's propulsion speed shows a decay that is slower than $\mu^{-1/2}$, which strongly suggests that the nematode does not swim with constant power. The maximum power generated by the organism is approximately 200 pW, calculated for $\mu = 30$ mPa · s.

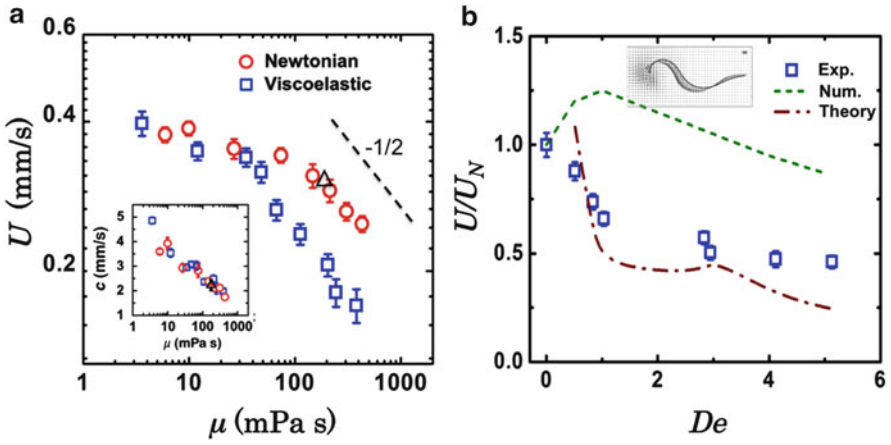

Fig. 7.13 (**a**) Nematode's swimming speed U as a function of shear viscosity μ for Newtonian (*red circle*) and viscoelastic (*blue square*) fluids. *Triangle symbol* represents the nonelastic xanthan gum solution. The data shows that fluid elasticity decreases the nematode's swimming speed when compared to a Newtonian fluid of same viscosity. For $\mu > 30\,\text{mPa}\cdot\text{s}$, the nematode's swimming speed decreases, indicating a limit in power for this type of organism. Inset in (**a**) shows the nematode's wave speed as a function of viscosity for all fluids. There is no apparent difference between the different fluids at a given viscosity value. (**b**) Normalized swimming speed as a function of the Deborah number. Experimental data is plot, together with numerical [89] and theoretical predictions [83]. Note that swimming speed decreases as De is increased

Importantly, the values of U for viscoelastic fluids are found to be 35 % lower than the Newtonian fluid of same shear viscosity (Fig. 7.13a). For example, the nematode's swimming speeds for the viscoelastic and Newtonian cases are 0.18 mm/s and 0.25 mm/s, respectively, even though the shear viscosity for both fluids is $300\,\text{mPa}\cdot\text{s}$ (Fig. 7.13a). The decrease in swimming speed in CMC (polymeric) solutions does not seem to be due to shear-thinning effects since nematode swimming in the non-viscoelastic, shear-thinning fluid (XG) showed no apparent decrease in propulsion speed (Fig. 7.13a, triangle symbol) compared to the Newtonian case. This result with XG is in agreement with the recent theoretical analysis of a waving sheet in a shear-thinning fluids [85].

So far, experiments using an undulatory, low Re swimmer (i.e., *C. elegans*) show that for similar viscosities fluid elastic stresses seem to hinder the organisms' propulsion speed. An important question is whether the organism is responding or adapting to the extra elastic stresses present in the fluid or are the polymer molecules toxic to the organism? In other words, is the observed decrease in swimming speed due to hydrodynamics or biology? This is a difficult question to answer with certainty, but one can address it at least in part by comparing the swimming phenotypic behavior (i.e., kinematics) between Newtonian and viscoelastic fluids. The wave speed c produced by the nematode is of particular interest since it has been shown that the values of c seem to change significantly once the nematode adopts a different swimming gait, i.e., swimming versus crawling [111]. The wave speed

can be easily measured from the curvature contour plots. The inset in Fig. 7.13a shows the nematode's bending wave speed c as a function of fluid viscosity. Results indicate that viscoelasticity (and polymer molecules) has negligible effect on the nematode's swimming kinematics. That is, the changes in kinematics including the decrease in beating frequency and wave speed are due to viscous effects only. In addition, there is no evidence of change in motility gait (e.g., swimming to crawling) as μ increases since the beating amplitudes remain constant ($A = 0.26\,\text{mm}$) even for the most viscous fluid ($\mu = 400\,\text{mPa}\cdot\text{s}$).

The effects of fluid elasticity on the nematode's swimming behavior are best illustrated by plotting the normalized swimming speed U/U_N as a function of the Deborah number ($\text{De} = \lambda f$), where U_N is the Newtonian speed. Figure 7.13b shows that the normalized swimming speed decreases monotonically with De and reaches an asymptotic value of 0.4 as De is further increased. In other words, as the elastic stresses increase in magnitude in the fluid, it introduces a larger resistance to propulsion, therefore decreasing the nematode's swimming speed.

Comparing Experiments to Calculations We can now compare the experimental results to the numerical and theoretical predictions discussed earlier. Of course, such comparisons are not quite fair because there are significant differences between the experiments and the calculations. For example, most calculations are two-dimensional (2D) and for small-amplitude displacements while the nematode is allowed to swim in 3D and can bend quite a bit. Most importantly, while the calculations assume prescribed kinematics or waveform, the nematode is free to choose its own. Nevertheless, qualitative assessments can be made.

We begin by noting that for all the experiments presented in this section, the ratio of the solvent viscosity to the total solution viscosity is below 0.05, which is similar to the calculations [83, 107]. As shown in Eq. (7.2), the swimming speed U of an undulating sheet is predicted to decrease with increasing De. While the experimental data supports the predicted trend, at least qualitatively, there are quantitative discrepancies between the experimental and theoretical results as shown in Fig. 7.13b. Some of the possible reasons for the observed discrepancies may be the finite length of the swimmer and the assumption of small beating amplitude in the theoretical works. That is, only small deflections are considered for both the waving sheet and cylinder while the nematode shows significant bending. Nevertheless, the theoretical models are able capture the main trends in the experimental data and perform surprisingly well.

How do the experimental results compare to the numerical simulations of Teran et al. [89]? Remember that the simulations predict an interesting enhancement of the sheet swimming speed at $\text{De} = 1$. The experimental results do not reveal such swimming speed enhancement, although a scale-up mechanical experiment did find such enhancement [90]. Nevertheless, for $\text{De} > 1$, the simulation predicts a gradual decrease in U as elasticity is increased. The discrepancies between the experiment and the simulations are most likely due to the difference in the swimming beating patterns. While simulations used a left-moving traveling wave with an amplitude that increased from head to tail, the experiments with *C. elegans* reveal a traveling

wave with an exponential decay from head to tail. Therefore, it is a bit unfair to directly compare the numerical simulations with the *C. elegans* work since the swimming kinematics are *very* different. As a side note, a recent three-dimensional numerical simulation of helical bodies in viscoelastic fluids by Spagnolie et al. [93] found that an enhancement in propulsion speed is indeed possible at $\mathrm{De} = 1$, in good agreement with scale-up experiments [90]. Clearly, swimming kinematics matter, and Chap. 10 provides an interesting discussion on the effects of swimming beating patterns on propulsion in viscoelastic fluids.

A Possible Mechanism: The Role of Extensional Viscosity So what could explain the decrease in swimming speed for nematodes moving in viscoelastic fluids? One possible explanation may be related to the *extensional viscosity* of polymeric fluids. The reader may be very familiar with the concept of shear viscosity μ, which is the fluid resistance to a shear deformation. The concept of extensional viscosity may be less familiar because it is not usually taught in standard fluid dynamics textbooks. Simply put, extensional viscosity η_e is the fluid resistance to an extensional deformation. Pure extensional flows are devoid of shear; such flows are often referred to as shear-free flows. Examples of shear-free flows also include biaxial stretching and elongation flows.

For Newtonian fluids, the extensional viscosity is equal to three times the shear viscosity such that $\eta_e = 3\mu$. This result was first reported by Trouton over a century ago in 1906 [112]. The quantity η_e/μ is often referred as the Trouton ratio; for Newtonian liquids, the Trouton ratio is constant ($\mathrm{Tr} = \eta_e/\mu = 3$). Viscoelastic fluids, however, can exhibit an enhancement in η_e compared to Newtonian fluids due to the extra elastic or polymeric stresses. Many experiments have shown that the extensional viscosity of liquids containing flexible polymers can be orders of magnitude larger than the extensional viscosity of Newtonian fluids [113, 114]. This is true even for viscoelastic and Newtonian fluids that have similar values of μ. In addition, while Newtonian fluids exhibit η_e values that are independent of strain, viscoelastic fluids show strain-hardening behavior. It should be evident that viscoelastic and Newtonian fluids will behave quite differently in flows with a strong extensional component [115].

But, how can extensional viscosity explain the reduced swimming speed of *C. elegans* in viscoelastic fluids? A clue may be in the velocity fields produced by the swimming nematodes. Figure 7.14 shows typical streamlines computed from experimentally measured velocity fields using particle-tracking methods for both the (a) Newtonian and (b) viscoelastic cases. Overall, the streamlines display large recirculation flow structures, or vortices, that are attached to the nematode's body. While the large-scale patterns are similar for both cases, detailed inspections shows the appearance of a distinct *hyperbolic point* near the nematode for the viscoelastic case. A recent computational effort by Guy and Thomases also found the existence of such hyperbolic points in the velocity fields of swimming nematodes (Fig. 10.9 in Chap. 10 of this book). It is important to note that a flow near such hyperbolic points is purely extensional. The hypothesis is that the decrease in U (in the nematode case, at least) is mostly likely due to the sudden increase of elastic stresses near the

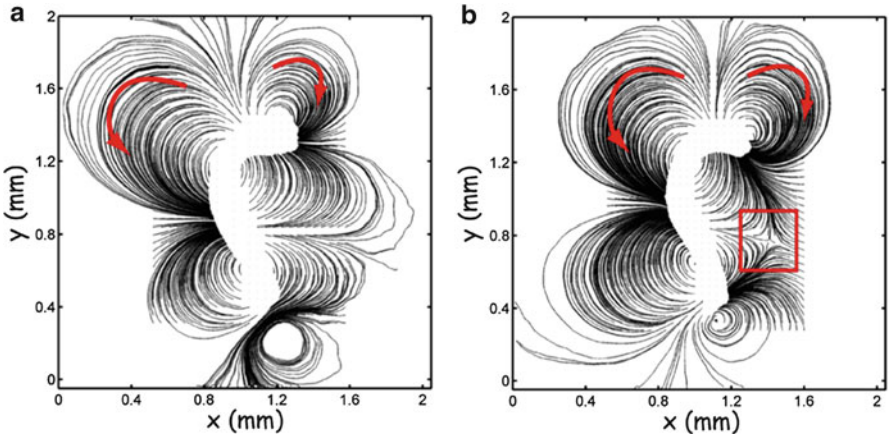

Fig. 7.14 (**a**) Streamlines computed from instantaneous velocity fields of Newtonian ($\mathrm{Re} < 10^{-3}$) and (**b**) polymeric ($\mathrm{Re} < 10^{-3}$; $\mathrm{De} = 3.0$) fluids. *Arrows* in (**a**, **b**) indicate the flow direction and the box in (**b**) shows a hyperbolic point in the flow

regions of high velocity gradients such as hyperbolic points. Near such regions, the extensional viscosity of a solution of flexible polymers can be orders of magnitude larger than a Newtonian fluid, resulting in an additional resistance to fluid transport and swimming.

In summary, experiments with the nematode *C. elegans* show that fluid elasticity can hinder its swimming speed. Further, it appears that the nematode's swimming speed decreases with increasing fluid elasticity, that is, U decreases as the Deborah number is increased. This trend is predicted by both numerical simulations [89, 93] and theory [83, 107], but the agreement is only qualitative. Hence, there is plenty of room for refining the experiments, theory, and simulations. It is clear that knowledge of the flow fields is important in determining how fluid elasticity (and other rheological properties) affects the organism's swimming kinematics and dynamics. In the case of complex fluids in particular, one is interested in the interactions between the fluid microstructure (e.g., polymer molecules, networks) and the flow fields produced by swimming microorganisms. (Of course different swimming kinematics usually result in different flow fields.) In the next section, we will discuss the undulatory swimming of *C. elegans* in non-dilute (i.e., semi-dilute and concentrated) solutions, where polymer networks rather than single molecules are of interest.

5.2.3 Swimming Experiments with *C. elegans*: Beyond the Dilute Regime

In this section, we will briefly discuss the swimming behavior of *C. elegans* in semi-dilute and concentrated polymeric solutions. Such solutions are characterized by the formation of polymer networks. The interplay between the fluid's internal structure

(e.g., polymer networks) and self-propulsion is critical to many biological processes such as reproduction [116], bacterial infection [117], and biodegradation in soil [118]. Early experimental observations have revealed that polymer networks can enhance the swimming speed of flagellated bacteria moving in solutions containing long-chain polymer molecules [119, 120]. For these small organisms ($L < 10\,\mu$m), it has been argued that the main mechanism for this propulsion enhancement is due to the benefits of pushing against a quasi-rigid polymer network [119, 121]. It is worth noting that the exact mechanism responsible for the observed propulsion enhancement is still not clear.

The role of the mechanical properties of fluid internal networks on an organism's swimming behavior has recently been investigated in numerical [121–124] and theoretical [125] studies. Numerical studies of swimming in structured fluids have postulated that the shapes and dynamics of internal networks are accounted for by two effective anisotropic viscosities [121, 124], which qualitatively explain some of the observed propulsion enhancement in microorganisms [119, 120]. Such anisotropic viscosities, however, are difficult to measure and apply to quantitative analysis. In heterogeneous, gel-like environments, modeled by embedding stationary objects in an incompressible viscous fluid, the swimming speed of a microorganism can be enhanced by the underlying structures in the fluid [125]. For internal networks made of small molecules, such as a binary blend of two intermixed fluids, a two-fluid model predicts an enhancement in swimming speed for stiff and compressible networks [122] and a reduction in swimming speed when local distributions of volume fractions of the two phases scale differently for thrust and drag [123]. Overall, the observed propulsion speed variations in these studies underscore the important role of the fluid internal structures on the swimming behavior of microorganisms.

But let's see how the fluid internal structures, in this case polymer networks, affect the swimming behavior of *C. elegans*; more details can be found elsewhere [126]. Polymer networks are formed by controlling the concentration of the biocompatible rodlike polymer xanthan gum (XG) in water. Polymer concentration ranges from 300 ppm to 5,000 ppm by weight. These XG solutions transition from the semi-dilute to the concentrated regime at a concentration of approximately 3,000 ppm [126]. This is made clear by plotting the solutions' zero-shear viscosity μ_0 as a function of polymer concentration, as shown in Fig. 7.15a. Note that the values of μ_0 increase as the polymer concentration c is increased, as expected. But we find a change in slope as the solution transitions from the semi-dilute to the concentrated regime at a concentration of approximately 2,800 ppm. This transition is commonly interpreted as a structural transition [127, 128]. In concentrated solution, the shape and dynamic properties of polymer networks dominate flow behaviors; in semi-dilute solution, the hydrodynamic interactions among individual polymers dominate flow behaviors [128].

Effects of Polymer Networks on Swimming Speed Fig. 7.15b shows that U remains relatively constant for polymer concentrations below 3,000 ppm. Surprisingly, however, the data shows sudden increase in U for concentrations above

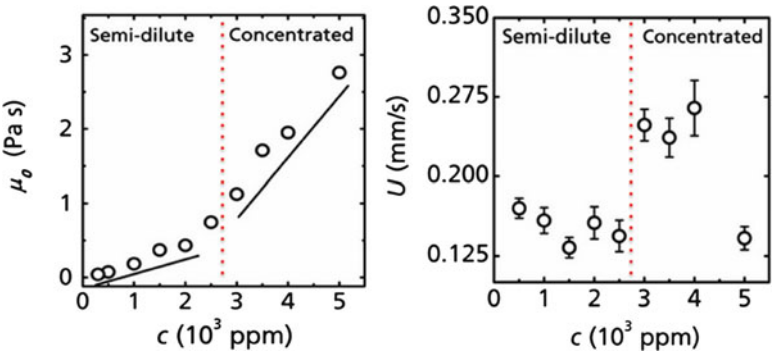

Fig. 7.15 (*Left*) Xanthan gum's (XG) zero-shear viscosity μ_0 as a function of polymer concentration c. The values of μ_0 increase with polymer concentration, as expected. The change in slope at $c \approx 2,800$ ppm is often associated with a structural transition. (*Right*) Nematode swimming speed U as a function of concentration. Swimming speed exhibits a rapid increase as the solution enters the concentrated regime at approximately 2,800 ppm

3,000 ppm. The values of U are maintained around 0.15 mm/s in semi-dilute solutions ($c < 2{,}800$ ppm), but they quickly rise by 65 % to about 0.25 mm/s in concentrated solutions ($c > 2{,}800$ ppm) *despite a significant increase in solution viscosity*. As expected, the swimming speed ultimately decreases as the concentration is further increased due to the nematode's finite power output [91]. A recent theoretical work suggests that such increase may be due to the presence of polymer networks in the media and that microorganisms may be able to push against such quasi-static networks and move more efficiently [121]. However, because of the large difference in length scales between the nematode (≈ 1 mm) and the polymer networks ($\approx 10\,\mu$m), this notion does not adequately explain the observed propulsion enhancement.

A possible explanation for this enhancement in U in concentrated solutions is given in [126], in which the authors argue that the phenomenon is most likely due to shear-induced fluid anisotropy. That is, the increase in U observed in Fig. 7.15b is probably due to the anisotropic response of the fluid microstructure to applied stress due to the nematode's swimming motion. In short, the undulatory swimming motion of *C. elegans* induces a structural anisotropy which leads to an increase in the effective drag coefficient ratio C_n/C_t (see RFT equation in Sect. 1) and consequently an enhancement in U.

The above results show that the nematode *C. elegans* can swim faster in concentrated solutions than in semi-dilute solutions. This is an unexpected result since the fluid viscosity increases as polymeric solution transitions from the semi-dilute to the concentrated regime. This sudden increase in U is thought to be connected to the anisotropic response of the fluid microstructure to applied shear stresses due the nematode's motion [126]. While intriguing, the proposed mechanism is speculative due to the difficulty to measure or visualize the polymer microstructure during swimming. In these cases, numerical simulations and theoretical calculations can provide much needed clarity and understanding to the problem.

5.2.4 Swimming Experiments with *C. elegans*: Final Remarks

In this section, we discussed the swimming behavior of the nematode *C. elegans* in Newtonian and viscoelastic (i.e., polymeric) fluids. For dilute polymeric solutions, experiments show that fluid elasticity hinders the swimming speed of nematodes by 40 % compared to Newtonian fluids. The swimming speed is also shown to decrease as elasticity (i.e., Deborah number) increases. On the other hand, for concentrated polymeric solutions, the presence of polymer networks seem to enhance swimming speed by as much as 65 % when compared to semi-dilute and dilute polymeric solutions. These results underscore the importance of the fluid microstructure and its interactions with the applied stresses generated by the swimmer. Perhaps the main message so far is that it is difficult to quantitatively describe a priori the motility of microorganisms in complex fluids without knowledge of the interactions between the fluid microstructure and the applied stresses. It becomes clear that these non-trivial interactions need to be accounted for in theoretical calculations and numerical simulations.

5.3 *Fluid-Assisted Locomotion in Complex Fluids: Artificial Swimmers*

As shown above, fluid elasticity can significantly affect the swimming behavior of live organisms. In this section, we will explore a different, and perhaps simpler, question: *Can fluid elasticity enable propulsion?*

To answer the above question, one needs to think back to the "scallop theorem," which tells us that only nonreciprocal deformations of the swimmer can break time-reversal symmetry and result in net motion [1]. The main assumptions of the theorem is that the swimmer is moving at low Reynolds numbers ($Re < 0.1$) and that the fluid is purely viscous or Newtonian. So, in order to break the "scallop theorem" or kinematic reversibility one needs to increase the amount of inertia in the system (i.e., increase Re) or alternatively use fluids that possess nonlinear rheological behavior. In this section, we will review recent experiments [92] in which artificial particles with reciprocal swimming strategies are able to break the scallop theorem once immersed in complex fluids. The experiments focus mainly on the role of viscoelasticity, and two main types of fluids will be used: (i) dilute polymeric solutions [92] and (ii) wormlike micellar (WLM) solutions [129].

Before we begin, it is worth noting that the possibility that fluid elasticity can *enable* rather than modify propulsion circumventing the scallop theorem is still largely unexplored. Propulsion enabled by fluid elasticity has been predicted for the three special cases of reciprocal motion: a flapping surface extending from a plane [130, 131]; a sphere which generates small-amplitude sinusoidal motion of fluid along its surface [8]; and a "wriggling" cylinder with reciprocal forward and backward strokes at different rates [88]. However, there remains little experimental demonstration, and such propulsion of free, finite-amplitude swimmers has been seldom studied.

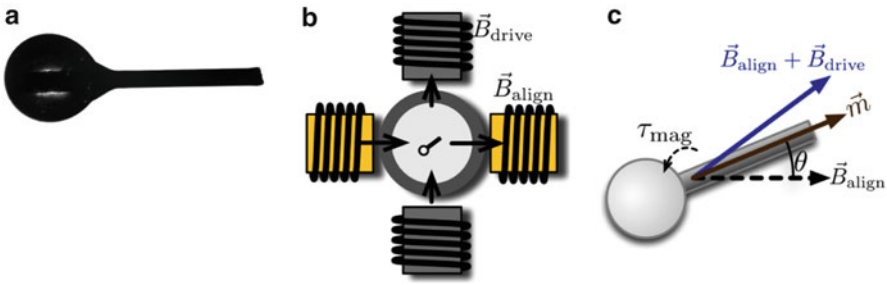

Fig. 7.16 (**a**) Snapshot of the polar dimer. An epoxy bead is attached to a steel wire to form polar (asymmetric) dimers. (**b**) *Top view* of the experiment. Two aligning electromagnets at constant current are orthogonal to two driving magnets, controlled by a computer. (**c**) The dimer with magnetization $\mathbf{m}$ experiences torque τ_{mag} to align with the magnetic field. Dimer orientation $\hat{a}$ oscillates around $\langle \hat{a} \rangle$, which is parallel to $\mathbf{B}_{\text{align}}$

5.3.1 Experiments with Reciprocal Swimmers: Can Fluid Elasticity Enable Propulsion?

Here, we briefly discuss recent experiments [92, 129] in which a single rigid object, in this case a dumbbell particle or dimer, is actuated in a reciprocal manner in very viscous fluids. In the experiments, the dimer such as the one shown in Fig. 7.16 is immersed in a fluid and repeatedly reoriented by a magnetic field. The effects of inertia are absent due to the high fluid viscosity ($\sim 10\,\text{Pa}\cdot\text{s}$), resulting in $\text{Re} \ll 0.1$ comparable to that of a swimming microorganism. By applying only magnetic torques, the apparatus reciprocally actuates just one degree of freedom in the system, the dimer's orientation $\hat{a}$. For a purely viscous Newtonian fluid at low Reynolds numbers, the authors found no net motion because $\hat{a}(t)$ is cyclic; this is as expected.

Experimental Setup Before diving into the discussion, let us briefly describe the experimental setup. More details can be found elsewhere [92, 129]. The artificial swimmer is a polar (asymmetric) dimer (Fig. 7.16a); symmetric dimers are also used for control but no net motion is expected. The polar dimer consists of a piece of carbon steel wire of length $2R_{\text{dimer}} = 2.5$–$3\,\text{mm}$ and diameter $230\,\mu\text{m}$, with an epoxy bead of diameter $2R_{\text{dimer}} \sim 500\,\mu\text{m}$ at one end. The dimer is then immersed in a fluid bath that is surrounded by four electromagnets; a schematic of the apparatus is shown in Fig. 7.16b. The dimer has orientation $\hat{a}$ and is magnetized with moment $\mathbf{m} = \hat{a}m$, so that a uniform magnetic field $\mathbf{B}$ reorients it with torque $\boldsymbol{\tau}_{\text{mag}} = \mathbf{m} \times \mathbf{B}$, as depicted in Fig. 7.16c.

Working Fluids The dimer is immersed in a container (50 mm tall, 30 mm in diameter) of either Newtonian or viscoelastic fluid (Fig. 7.16b). The Newtonian fluid is a 96 %-corn syrup aqueous solution (by mass) with a kinematic viscosity μ/ρ of approximately 4×10^4 cSt. Two viscoelastic solutions are prepared: a dilute polymeric solution and a WLM solutions. The polymeric solution is made by adding 0.17 % (by mass) of high-molecular-weight polyacrylamide (PAA, $M_W = 1 \times 10^6$)

to a viscous Newtonian solvent (93 %-corn syrup aqueous solution). The solution has nearly constant shear viscosity of approximately 50Pa · s and a relaxation time λ of approximately 2 s.

The WLM solution is prepared by slowly adding 130 mM hexadecyltrimethylammonium bromide (CTAB) to an aqueous solution of 130 mM sodium salicylate (NaSal). This type of WLM solutions is known to form long wormlike micelles that continuously break and reform due to thermal fluctuations leading to viscoelastic stress relaxation. The relaxation time λ of the WLM solution is approximately 1.5 s [129]. Here, the Deborah number is defined as $\mathrm{De} f_{\mathrm{drive}} \lambda$.

Swimming with Reciprocal Motion Now that the methods are in place, we can ask an important question: Can the nonlinear rheological properties of a given fluid enable propulsion at low Re? Before we discuss the results, it is worth making sure that artifacts that could lead to net motion are not being introduced in the experiment. To that end, the investigators [129] calibrated their results against a polar and symmetrical dimer immersed in a viscous Newtonian fluid with similar shear viscosity as the polymeric and WLM solutions. As shown in Fig. 7.17a, they found negligible net displacement, comparable to the effects of magnetic drift and sedimentation when driving is turned off altogether.

Evidence of purely elastic propulsion is shown in Fig. 7.17b–d for the polar dimer immersed in dilute polymeric (b) and WLM solutions (c, d). Overall, the data show a striking contrast between performing reciprocal motion in Newtonian and in complex, viscoelastic fluids. For example, Fig. 7.17b shows that in dilute polymeric solutions, far from any boundaries, the polar dimer at $\mathrm{De} = 5.7 (f_{\mathrm{drive}} = 2.8\,\mathrm{Hz}; \mathrm{Re} = 1.2 \times 10^{-4})$ is able to achieve net motion at constant speed even under reciprocal forcing. The same is true for the WLM solution (Fig. 7.17b, d). It is interesting to note that, unlike the polymeric solution case, the swimming direction in the WLM solutions seems to depend on De. For low elasticity values ($\mathrm{De} < 1$), the particle moves towards the bead while the particle moves preferentially towards the rod for cases in which actuating frequency is approximately similar to the fluid relaxation time ($\mathrm{De} \sim 1$). The dimer directional dependence on De in WLM solutions is still not understood.

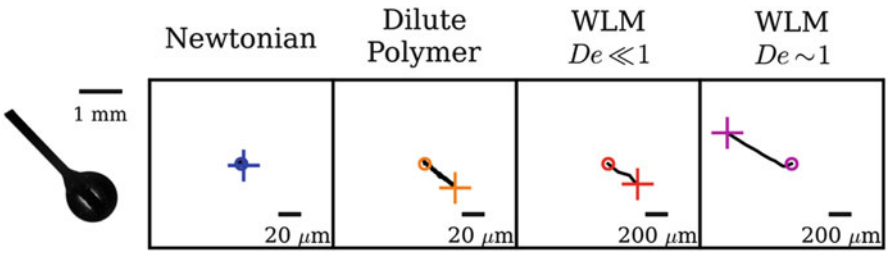

Fig. 7.17 Centroid trajectories from ○ to + reciprocally actuated polar dimer (*leftmost panel*) in Newtonian, dilute polymeric, and wormlike micellar (WLM) solutions at low and high Deborah numbers. No appreciable net motion is found in the Newtonian case. Appreciable net motion is found once small amounts of polymers or surfactants (WLM) are added to a Newtonian solvent

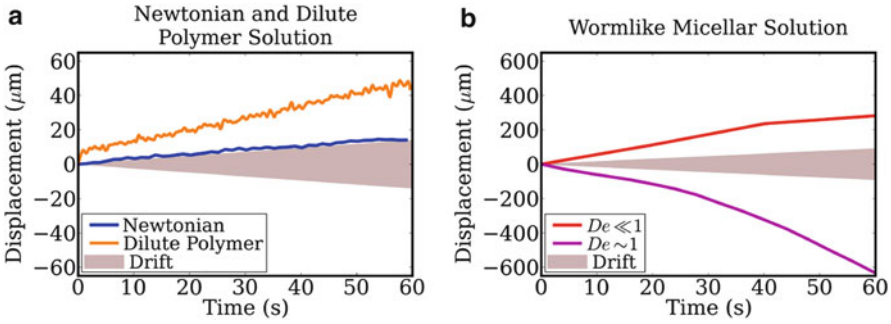

Fig. 7.18 Dimer net displacement as a function of time. The reciprocally actuated dimer is immersed in (**a**) polymeric and (**b**) wormlike micellar solutions. *Shaded areas* correspond to the dimer drift due to small but finite magnetic gradients

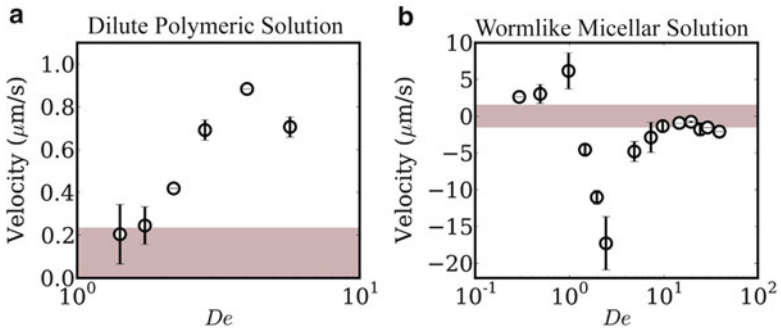

Fig. 7.19 Dependence of mean propulsion velocity on Deborah (De) for a reciprocally actuated dimer immersed in (**a**) dilute polymeric and (**b**) wormlike micellar (WLM) solutions

Figure 7.18a, b shows the net displacement for the dilute polymeric and WLM solutions, respectively. Both cases show dimer displacements well above the noise or drift level (shaded area). Clearly, a much larger displacement can be achieved with the WLM solutions, although the mechanisms are still unknown. The data also shows that the dimer can move either towards the bead (positive velocity) or towards the rod (negative velocity) depending on the De as discussed above.

In order to gain further understanding on the effects of fluid elasticity on the dimer motion, it is helpful to plot the displacement data as a function of De. Figure 7.19a, b shows the dimer velocity as a function of De for the dilute polymeric and WLM solutions, respectively. Recall that the positive velocity means that the polar dimer is moving towards its bead and negative velocity means that the dimer is moving towards its rod. For the polymeric solution case, the velocity increases monotonically as a function of De. In fact, the velocity seems to obey a De^2 scaling.

The effects of elasticity are less obvious for the WLM solutions. While it is clear that the polar dimer speed increases as De increases, the velocity trend is more complex. It seems that for low elasticity values ($0 < De < 1$, the trend and dimer

swimming direction resemble the polymeric solution data. For De ≥ 1, the dimer swimming direction reverses, and for De $\gg 1$ the dimer comes to a complete stop. While the exact mechanisms leading to such behaviors in WLM solutions are not well understood, the data underscore the rich nonlinear behavior encountered in complex fluids.

In summary, we find that polar particles (dimers) undergoing reciprocal motion can indeed achieve locomotion at low Reynolds numbers in complex, viscoelastic fluids. This is fascinating because it opens the door for a new way to achieve locomotion, one that relies on the fluid itself. For the case of dilute polymeric solutions, the net motion achieved by the dimers results from elastic stresses due to flow-induced changes in polymer conformation. These elastic stresses are history-dependent and do not entirely cancel out over one forcing period, but instead have a small rectified component that accumulates. In fact, Keim and Arratia [92] claim that the combination of the fluid first normal stress difference N_1 and the curved streamlines produced by the actuated dimer leads to a volume force (or "hoop stress") that is able to displace the dimer. The proposed mechanism is reasonable but it is yet to be validated. The picture is less clear for WLM solutions where shear-bands are known to occur in addition to elasticity.

Finally, this type of work is a proof-of-concept for an artificial "swimmer" that moves through complex fluids with only reciprocal actuation, a simple body shape, and no moving parts—a less complicated design than for other propulsive strategies [47, 132]. There may thus be a practical route to studies of collective phenomena among large numbers of such particles. These principles could also be applied to microfluidic pumps [130, 131] or to exploiting other types of nonlinear fluid rheology. Further understanding of this effect and similar ones could greatly simplify fabrication of microswimmers for many artificial environments or for biological settings where viscoelasticity is ubiquitous.

6 Conclusions and Outlook

In this chapter, we discussed swimming in complex fluids. The discussion was given from an experimental point of view and was centered on a few fundamental experiments both in living and in artificial systems that we hope illustrate the rich dynamics encountered by organisms moving in complex fluids, particularly in viscoelastic fluids. Much of the investigations in viscoelastic fluids was driven by a simple question: does elasticity hinder or enhance swimming speed?

Theoretical analysis on idealized swimming models, following the seminal work of Taylor [27], showed that in general fluid elasticity hinders propulsion [83, 107]. Numerical simulations [89, 93], however, found that fluid elasticity could in fact enhance propulsion under certain conditions (De ~ 1). Experiments [90,91] seem to confirm such predictions, at least qualitatively. For example, the swimming speed of *C. elegans* effectively decreases once the organism is immersed in dilute viscoelastic

fluids, while propulsion speed increased for De ~ 1 in scale-up mechanical experiments with helical bodies. In more concentrated polymeric solutions, the nematode *C. elegans* showed a remarkable increase in speed for solutions possessing polymer networks. (There are of course many other impressive experimental investigations of swimming in anisotropic media such as liquid crystals [133–135] that could not be covered here.) Overall we find that it is very hard to know a priori whether fluid elasticity enhances or hinders the propulsion speed of microorganisms. In fact, it may be an unfair question altogether as the answer depends on the type of swimming kinematics (i.e., waveform) and the interactions of the swimmer with the fluid microstructure (i.e., polymer or particles). That is, the local details may matter quite a bit. Nevertheless, it is clear from both experiments and simulations that fluid elasticity can significantly affect the motility behavior of microorganisms.

Parallel to these considerations, we also discussed an exciting avenue of new developments, that is, the possibility of fluid-assisted propulsion. This type of propulsion is driven by the nonlinear rheological properties of the fluid such as viscoelasticity and formation of shear-bands. We showed that even for reciprocally actuated polar particles, the extra elastic stresses of polymeric fluids can lead to net motion at low Reynolds numbers. It is important to note that under the same conditions, the same particle in a Newtonian fluid achieves no net motion due to kinematic reversibility. These findings are exciting because such discovery opens a new mechanism for the study of "active" particles and collective behavior in complex fluids.

So where do we go from here? Of course there is still much to be done and understood. The question of how microorganisms move in complex fluids is still largely unanswered. We still do not know how microorganisms move in rheologically complex materials that possess rate-dependent viscosity, yield stress, and thixotropy. But a picture is starting to emerge, and it seems that the interaction of the swimmer with the fluid microstructure is very important. That is not surprising since microorganisms with different swimming kinematics will likely produce different velocity fields in a given fluid, and the bulk response will be determined by the way the fluid microstructure interacts with the velocity field. For example, it is well known that extensional flows are more efficient in stretching and aligning polymer molecules than shear flows, and swimmers that produce flows with a large extensional component are dominated by the fluid extensional viscosity. On the other hand, swimmers that produce large amounts of curvature may experience a viscoelastic instability due to hoop stresses. So knowledge of the velocity field is quite important, but equally important is how the molecules or particles respond to the imposed velocity field. In a way, the swimmer may be thought of as a local probe for fluid rheology. An exciting and important direction that would allow us to gain a more complete understanding of swimming in complex fluids is to determine how single polymer molecules, particles, and networks interact with microorganisms. This direction will ultimately take us from the continuum to a statistical mechanics description of the problem. The challenge lies in connecting the statistical representation with the continuum (bulk) description.

Finally, one can also ask the question of how multiple swimmers interact in complex fluids. One would anticipate that the fluid microstructure will significantly alter the way multiple microorganisms interact. The type of work is related to the field of active matter or fluid in which "active" or live particles are present in the fluid medium. Active fluids differ from their passive counterpart in that the active particles have the ability to absorb and dissipate energy and to generate motion and mechanical stresses in the fluid medium (see Chap. 9). Importantly, these active particles can drive the system out of equilibrium even in the absence of external forcing. Active fluids exhibit novel properties not seen in conventional (passive) complex fluids such as large-scale flows and collective motion on length scales much greater than the particle dimensions [136], anomalous shear viscosity [137], giant density fluctuations [138], and enhanced fluid mixing [139]. While much recent progress has been made, the dynamics and flow behavior (rheology) of such active complex fluids are still poorly understood. In this case, one can take advantage of a vast body of knowledge developed to understand passive complex fluids.

Acknowledgment The authors would like to thank David Gagnon, Nathan Keim, Arvind Gopinath, Alexander Leshansky, and Xiaoning Shen for help with the text and in drafting illustrations. This work was supported by the US-Israel Binational Science Foundation (BSF grant nr. 2011323) and J. Sznitman was supported in part by the European Commission (FP7 Program) through a Career Integration Grant (PCIG09-GA-2011-293604). P.E. Arratia was supported in part by the Army Research Office through award W911NF-11-1-0488 and by NSF-CBET-Career Award.

References

1. E.M. Purcell, Am. J. Phys. **45**, 3 (1977)
2. C. Brennen, H. Winet, Annu. Rev. Fluid Mech. **9**(1), 339 (1977)
3. J. Gray, J. Exp. Biol. **32**(4), 775 (1955)
4. J. Gray, G. Hancock, J. Exp. Biol. **32**(4), 802 (1955)
5. N. Cohen, J.H. Boyle, Contemp. Phys. **51**(2), 103 (2010)
6. J. Gray, H.W. Lissmann, J. Exp. Biol. **41**(1), 135 (1964)
7. J. Sznitman, X. Shen, R. Sznitman, P.E. Arratia, Phys. Fluids (1994–present) **22**, 121901 (2010)
8. E. Lauga, T.R. Powers, Rep. Prog. Phys. **72**(9), 096601 (2009)
9. J. Lighthill, SIAM Rev. **18**(2), 161 (1976)
10. N.A. Croll, *The Behaviour of Nematodes: Their Activity, Senses and Responses* (Edward Arnold, London, 1970)
11. J.G. White, E. Southgate, J.N. Thomson, S. Brenner, Philos. Trans. R. Soc. Lond. B Biol. Sci. **314**, 1 (1986)
12. W.B. Wood, *The Nematode Caenorhabditis elegans* (Cold Spring Harbour Laboratory, New York, 1987)
13. H.C. Berg, *E. coli in Motion* (Springer, New York, 2004)
14. H.C. Berg, Phys. Today **53**(1), 24 (2000)
15. H.C. Berg, Biochemistry **72**(1), 19 (2003)
16. H.C. Berg, Curr. Biol. **18**(16), R689 (2008)
17. D. Bray, *Cell Movements: From Molecules to Motility* (Garland Science, New York, 2001)

18. D.R. Mitchell, J. Phycol. **36**, 261 (2000)
19. M. Werner, L.W. Simmons, Biol. Rev. **83**, 191 (2008)
20. I. Gibbons, J. Cell Biol. **91**(3), 107s (1981)
21. R. Lyons, O. Djahanbakhch, T. Mahmood, E. Saridogan, S. Sattar, M. Sheaff, A. Naftalin, R. Chenoy, Hum. Reprod. **17**, 584 (2002)
22. R. Lyons, E. Saridogan, O. Djahanbakhch, Hum. Reprod. Update **12**, 363 (2006)
23. T. Nakahari, A. Nishimura, C. Shimamoto, A. Sakai, H. Kuwabara, T. Nakano, S. Tanaka, Y. Kohda, H. Matsumura, H. Mori, Biomed. Res. **32**, 321 (2011)
24. P. Satir, M.A. Sleigh, Annu. Rev. Physiol. **52**, 137 (1990)
25. A. Korngreen, Z. Priel, Biophys. J. **67**(1), 377 (1994)
26. A.L. Oldenburg, R.K. Chhetri, D.B. Hill, B. Button, Biomed. Opt. Express **3**, 1978 (2012)
27. G. Taylor, Proc. R. Soc. Lond. Ser. A Math. Phys. Sci. **209**, 447 (1951)
28. G. Taylor, Proc. R. Soc. Lond. Ser. A Math. Phys. Sci. **211**, 225 (1952)
29. I. Aranson, Physics **6**, 61 (2013)
30. J.S. Guasto, R. Rusconi, R. Stocker, Annu. Rev. Fluid Mech. **44**, 373 (2012)
31. S. Chattopadhyay, R. Moldovan, C. Yeung, X. Wu, Proc. Natl. Acad. Sci. **103**(37), 13712 (2006)
32. D. Katz, J. Blake, S. Paveri-Fontana, J. Fluid Mech. **72**(03), 529 (1975)
33. J. Happel, H. Brenner, *Low Reynolds Number Hydrodynamics: With Special Applications to Particulate Media*, vol. 1 (Springer, Berlin, 1983)
34. D. Saintillan, Physics **3**, 84 (2010)
35. S.A. Koehler, T.R. Powers, Phys. Rev. Lett. **85**(22), 4827 (2000)
36. B. Qian, T.R. Powers, K.S. Breuer, Phys. Rev. Lett. **100**, 078101 (2008)
37. S.Y. Tony, E. Lauga, A. Hosoi, Phys. Fluids (1994–present) **18**, 091701 (2006)
38. M.S. Sakar, C. Lee, P.E. Arratia, Phys. Fluids **21**, 91107 (2009)
39. S. Zhong, K.W. Moored, V. Pinedo, J. Garcia-Gonzalez, A.J. Smits, Exp. Therm. Fluid Sci. **46**, 1 (2013)
40. M. Kim, J.C. Bird, A.J. Van Parys, K.S. Breuer, T.R. Powers, Proc. Natl. Acad. Sci. **100**(26), 15481 (2003)
41. M.J. Kim, M.J. Kim, J.C. Bird, J. Park, T.R. Powers, K.S. Breuer, Exp. Fluids **37**(6), 782 (2004)
42. E. Setter, I. Bucher, S. Haber, Phys. Rev. E **85**, 066304 (2012)
43. P. Weiss, Sci. News **169**, 107 (2006)
44. R. Trouilloud, S.Y. Tony, A. Hosoi, E. Lauga, Phys. Rev. Lett. **101**, 048102 (2008)
45. C.H. Wiggins, D. Riveline, A. Ott, R.E. Goldstein, Biophys. J. **74**, 1043 (1998)
46. M. Leoni, J. Kotar, B. Bassetti, P. Cicuta, M.C. Lagomarsino, Soft Matter **5**(2), 472 (2009)
47. J.J. Abbott, K.E. Peyer, M.C. Lagomarsino, L. Zhang, L. Dong, I.K. Kaliakatsos, B.J. Nelson, Int. J. Rob. Res. **28**(11), 1434 (2009)
48. H.C. Berg, Rev. Sci. Instrum. **42**(6), 868 (1971)
49. H.C. Berg, Adv. Opt. Elect. Microsc. **7**, 1 (1978)
50. H.C. Berg, D.A. Brown, Nature **239**(5374), 500 (1972)
51. L. Turner, W.S. Ryu, H.C. Berg, J. Bacteriol. **182**, 2793 (2000)
52. S.C. Lenaghan, C.A. Davis, W.R. Henson, Z. Zhang, M. Zhang, Proc. Natl. Acad. Sci. **108**(34), E550 (2011)
53. K. Drescher, K.C. Leptos, R.E. Goldstein, Rev. Sci. Instrum. **80**(1), 014301 (2009)
54. E. Lauga, W.R. DiLuzio, G.M. Whitesides, H.A. Stone, Biophys. J. **90**(2), 400 (2006)
55. R. Di Leonardo, D. Dell'Arciprete, L. Angelani, V. Iebba, Phys. Rev. Lett. **106**(3), 038101 (2011)
56. A.P. Berke, L. Turner, H.C. Berg, E. Lauga, Phys. Rev. Lett. **101**(3), 038102 (2008)
57. J. Cosson, P. Huitorel, C. Gagnon, Cell Motil. Cytoskeleton **54**(1), 56 (2003)
58. L. Rothchild, Nature **198**, 1221 (1963)
59. D. Woolley, Reproduction **126**, 259 (2003)
60. S. Jana, S.H. Um, S. Jung, Phys. Fluids (1994–present) **24**(4), 041901 (2012)

61. P. Denissenko, V. Kantsler, D.J. Smith, J. Kirkman-Brown, Proc. Natl. Acad. Sci. **109**(21), 8007 (2012)
62. R. Ghosh, J. Sznitman, J. Vis. **15**, 1–3 (2012)
63. F. Lebois, P. Sauvage, C. Py, O. Cardoso, B. Ladoux, P. Hersen, J.M. Di Meglio, Biophys. J. **102**(12), 2791 (2012)
64. K. Konig, L. Svaasand, Y. Liu, G. Sonek, P. Patrizio, Y. Tadir, M. Berns, B. Tromberg, Cell. Mol. Biol. (Noisy-le-Grand, France) **42**(4), 501 (1996)
65. Y. Tadir, W. Wright, O. Vafa, T. Ord, R. Asch, M. Berns, Fertil. Steril. **53**, 944 (1990)
66. Z. Teff, Z. Priel, L.A. Gheber, Biophys. J. **92**, 1813 (2007)
67. S. Chattopadhyay, X.L. Wu, Biophys. J. **96**(5), 2023 (2009)
68. B. Rodenborn, C.H. Chen, H.L. Swinney, B. Liu, H. Zhang, Proc. Natl. Acad. Sci. **110**, E338 (2013)
69. G. Batchelor, J. Fluid Mech. **44**(03), 419 (1970)
70. A.T. Chwang, T. Wu, J. Fluid Mech. **67**(04), 787 (1975)
71. J.B. Keller, S.I. Rubinow, J. Fluid Mech. **75**(04), 705 (1976)
72. R.E. Johnson, J. Fluid Mech. **99**(02), 411 (1980)
73. J. Higdon, J. Fluid Mech. **90**(04), 685 (1979)
74. J. Higdon, J. Fluid Mech. **94**(02), 331 (1979)
75. H. Kurtuldu, D. Tam, A. Hosoi, K. Johnson, J. Gollub, Phys. Rev. E **88**(1), 013015 (2013)
76. S.T. Wereley, C.D. Meinhart, Annu. Rev. Fluid Mech. **42**, 557 (2010)
77. D. Murphy, D. Webster, J. Yen, Limnol. Oceanogr. Methods **10**, 1096 (2012)
78. K. Drescher, R.E. Goldstein, N. Michel, M. Polin, I. Tuval, Phys. Rev. Lett. **105**(16), 168101 (2010)
79. J.S. Guasto, K.A. Johnson, J.P. Gollub, Phys. Rev. Lett. **105**(16), 168102 (2010)
80. L.J. Fauci, R. Dillon, Annu. Rev. Fluid Mech. **38**, 371 (2006)
81. S. Suarez, H. Ho, Reprod. Domest. Anim. **38**, 119 (2003)
82. E.R. Trueman, *Locomotion of Soft-Bodied Animals* (Edward Arnold, London, 1975)
83. E. Lauga, Phys. Fluids **19**(8), 083104 (2007)
84. T.D. Montenegro-Johnson, D.J. Smith, D. Loghin, Phys. Fluids (1994–present) **25**, 081903 (2013)
85. J.R. Vélez-Cordero, E. Lauga, J. Non-Newtonian Fluid Mech. **199**, 37 (2013)
86. D. Katz, R. Mills, T. Pritchett, J. Reprod. Fertil. **53**(2), 259 (1978)
87. T. Chaudhury, J. Fluid Mech. **95**(01), 189 (1979)
88. H.C. Fu, C.W. Wolgemuth, T.R. Powers, Phys. Fluids **21**(3), 033102 (2009)
89. J. Teran, L. Fauci, M. Shelley, Phys. Rev. Lett. **104**, 038101 (2010)
90. B. Liu, T.R. Powers, K.S. Breuer, Proc. Natl. Acad. Sci. **108**, 19516 (2011)
91. X. Shen, P.E. Arratia, Phys. Rev. Lett. **106**, 208101 (2011)
92. N.C. Keim, M. Garcia, P.E. Arratia, Phys. Fluids (1994–present) **24**(8), 081703 (2012)
93. S.E. Spagnolie, B. Liu, T.R. Powers, Phys. Rev. Lett. **111**, 068101 (2013)
94. R.B. Bird, R.C. Armstrong, O. Hassager, *Dynamics of Polymeric Liquids. Vol. 1: Fluid Mechanics* (Wiley, New York, 1987)
95. R.G. Larson, *The Structure and Rheology of Complex Fluids*, vol. 4 (Oxford University Press New York, 1999)
96. E.S. Shaqfeh, Annu. Rev. Fluid Mech. **28**, 129 (1996)
97. H.C. Ho, S.S. Suarez, Reproduction **122**(4), 519 (2001)
98. D. Katz, T. Bloom, R. Bondurant, Biol. Reprod. **25**(5), 931 (1981)
99. L.A. McPartlin, S.S. Suarez, C.A. Czaya, K. Hinrichs, S. Bedford-Guaus, Biol. Reprod. **81**, 199 (2009)
100. A. Houry, M. Gohar, J. Deschamps, E. Tischenko, S. Aymerich, A. Gruss, R. Briandet, Proc. Natl. Acad. Sci. **109**(32), 13088 (2012)
101. S. Yazdi, A.M. Ardekani, Biomicrofluidics **6** (2012)
102. S. Jung, A.G. Winter, A. Hosoi, Int. J. Non-Linear Mech. **46**(4), 602 (2011)
103. A.G. Winter, R.L. Deits, A.E. Hosoi, J. Exp. Biol. **215**, 2072 (2012)
104. G.R. Fulford, D.F. Katz, R.L. Powell, Biorheology **35**(4), 295 (1998)

105. M.J. Kim, K.S. Breuer, Small **4**(1), 111 (2008)
106. D. Boger, J. Non-Newtonian Fluid Mech. **3**(1), 87 (1977)
107. H.C. Fu, T.R. Powers, C.W. Wolgemuth, Phys. Rev. Lett. **99**(25), 258101 (2007)
108. S.K. Lai, Y.Y. Wang, D. Wirtz, J. Hanes, Adv. Drug Deliv. Rev. **61**(2), 86 (2009)
109. S. Brenner, Genetics **77**(1), 71 (1974)
110. L. Byerly, R. Cassada, R. Russell, Dev. Biol. **51**(1), 23 (1976)
111. X. Shen, J. Sznitman, P. Krajacic, T. Lamitina, P. Arratia, Biophys. J. **102**, 2772 (2012)
112. F.T. Trouton, Proc. R. Soc. London Ser. A **77**, 426 (1906)
113. S.L. Anna, G.H. McKinley, J. Rheol. (1978–present) **45**(1), 115 (2001)
114. G.H. McKinley, T. Sridhar, Annu. Rev. Fluid Mech. **34**, 375 (2002)
115. P.E. Arratia, C. Thomas, J. Diorio, J.P. Gollub, Phys. Rev. Lett. **96**(14), 144502 (2006)
116. D.S. Guzick, J.W. Overstreet, P. Factor-Litvak, C.K. Brazil, S.T. Nakajima, C. Coutifaris, S.A. Carson, P. Cisneros, M.P. Steinkampf, J.A. Hill, New England J. Med. **345**(19), 1388 (2001)
117. C. Josenhans, S. Suerbaum, Int. J. Med. Microbiol. **291**(8), 605 (2002)
118. M. Alexander, *Introduction to Soil Microbiology* (Wiley, New York, 1991)
119. H.C. Berg, L. Turner, Nature **278**, 349 (1979)
120. W.R. Schneider, R. Doetsch, J. Bacteriol. **117**, 696 (1974)
121. Y. Magariyama, S. Kudo, Biophys. J. **83**, 733 (2002)
122. H.C. Fu, V.B. Shenoy, T.R. Powers, EPL (Europhys. Lett.) **91**(2), 24002 (2010)
123. J. Du, J.P. Keener, R.D. Guy, A.L. Fogelson, Phys. Rev. E **85**(3), 036304 (2012)
124. S. Nakamura, Y. Adachi, T. Goto, Y. Magariyama, Biophys. J. **90**, 3019 (2006)
125. A. Leshansky, Phys. Rev. E **80**(5), 051911 (2009)
126. D. Gagnon, X. Shen, P. Arratia, EPL (Europhys. Lett.) **104**(1), 14004 (2013)
127. A. Rodd, D. Dunstan, D. Boger, Carbohydr. Polym. **42**, 159 (2000)
128. M. Doi, *The Theory of Polymer Dynamics* (Oxford university press, Oxford, 1988)
129. D.A. Gagnon, N.C. Keim, X. Shen, P.E. Arratia, Fluid-induced propulsion of rigid particles in wormlike micellar solutions. Phys. Fluids **26**, 103101 (2014)
130. T. Normand, E. Lauga, Phys. Rev. E **78**, 061907 (2008)
131. O.S. Pak, T. Normand, E. Lauga, Phys. Rev. E **81**, 036312 (2010)
132. R. Dreyfus, J. Baudry, M.L. Roper, M. Fermigier, H.A. Stone, J. Bibette, Nature **437**(7060), 862 (2005)
133. S. Zhou, A. Sokolov, O.D. Lavrentovich, I.S. Aranson, Proc. Natl. Acad. Sci. **111**, 1265 (2014)
134. P.C. Mushenheim, R.R. Trivedi, H.H. Tuson, D.B. Weibel, N.L. Abbott, Soft Matter **10**, 88 (2014)
135. A. Kumar, T. Galstian, S.K. Pattanayek, S. Rainville, Mol. Cryst. Liq. Cryst. **574**(1), 33 (2013)
136. L.H. Cisneros, R. Cortez, C. Dombrowski, R.E. Goldstein, J.O. Kessler, Exp. Fluids **43**(5), 737 (2007)
137. A. Sokolov, I.S. Aranson, Phys. Rev. Lett. **103**, 148101 (2009)
138. V. Narayan, S. Ramaswamy, N. Menon, Science **317**, 105 (2007)
139. H. Kurtuldu, J.S. Guasto, K.A. Johnson, J.P. Gollub, Proc. Natl. Acad. Sci. **108**(26), 10391 (2011)